

ARTICLE TYPE

Optimal deployment of indoor wireless local area networks

Antoine Oustry*^{1,3} | Marion Le Tilly² | Thomas Clausen³ | Claudia D'Ambrosio³ | Leo Liberti³¹Ecole des ponts ParisTech,
Champs-sur-Marne, France²Ecole polytechnique fédérale de
Lausanne, Lausanne, Switzerland³LIX CNRS, École polytechnique,
Institut Polytechnique de Paris,
F-91128 Palaiseau, France

Correspondence

*Antoine Oustry. Email:
antoine.oustry@polytechnique.org

Abstract

We present a two-phase methodology to address the problem of optimally deploying indoor wireless local area networks. In the first phase, we use Helmholtz's equation to simulate electromagnetic fields in a typical environment such as an office floor. The linear system which results from the discretization of this partial differential equation is solved with a state-of-the-art library for sparse linear algebra. In the second phase, we formulate the network deployment problem in the setting of Binary Linear Programming. This formulation employs the simulator output as input parameters, and jointly optimizes the number of Access Points, their locations, and their emission channels. We prove that this optimization problem is NP-Hard, and use mathematical programming based techniques and heuristics to solve it. We present numerical experiments on medium-sized buildings.

KEYWORDS:

Wireless Networks; Indoor Radio Wave Simulation; Finite Difference Schema; Mixed-Integer Linear Programming; Relaxation; Heuristics; Frequency Assignment

1 | INTRODUCTION

Optimization problems related to Wireless Networks deployment have attracted considerable interest in the Operations Research (OR) and Mathematical Programming (MP) literature, especially since the 1990s. A particularly important problem, that of optimally deploying a Wireless Local Area Network (WLAN) in indoor environments, was mostly studied in the literature from the more technological point of view of computer networks, rather than using the algorithmic approaches afforded by OR/MP methods. This paper intends to bring the benefits of OR/MP to the Optimal WLAN Deployment (OWLD) problem. We note that the input data for the OWLD should be a precise description of the electromagnetic field at every point of the volume of interest. The approach proposed in this paper estimates the field intensity from a solution of the [partial](#) differential equations of the field.

1.1 | OR methods in wireless networks

We first provide a minimal survey of the impact of the OR/MP culture in some optimization problems related to wireless networks. The earliest models for radio network planning were related to the Minimum Dominating Set (MDS) problem [1]. More realistic and application-specific models followed, opening different research subdomains depending on the targeted application.

- Wireless Sensor Networks (WSN) are a set of spatially distributed sensors collecting and exchanging data and recording physical conditions [2]. The Relay Node Placement (RNP) problem is one of the major questions arising in the design of WSN. Connectivity being necessary for flow routing, RNPs are related to fundamental problems such as Minimum Connected Dominating Set (MCDS) [3], Minimum Steiner Tree (MST) [4, 5], and their variants [6, 7, 8]. In particular, finding the maximal data-rate of wireless connections subject to edge capacities leads to the Edge Capacitated MST [9]. More technological and applied works focus on deployment processes improving network performance [10], lifetime [11, 12], and energy-efficiency [13].

- The Frequency Assignment Problem (FAP) is the problem of assigning a frequency to each emitter of a wireless network while maximizing the Quality of Service (QoS) [14]. According to [15], "the FAP is probably the telecommunication application which has attracted the largest attention in the OR literature, both for its practical relevance and for its immediate relation to classical combinatorial optimization problems". Depending on technological objective and constraints, the FAP may assume very different forms. The main variants of this problem are Maximum Service FAP, the Minimum Order FAP, the Minimum Span FAP, and the Minimum Interference FAP [14].
- The Universal Mobile Telecommunications System (UMTS) is a mobile cellular system for networks based on the GSM standard. Due to the large operational cost for the mobile service operators, there is a huge need of optimizing at regional scale the base stations locations and configurations. This requires solving problems related to frequency assignment, emission power, antenna height/tilt/orientation, and more. The first models were simplified and based on the MDS [1] and the Capacitated Facility Location (CFL) [16] problems. In the 2000s, much work has been carried out in order to jointly optimize the location and configuration of the base stations using MP tools [17, 18, 19, 20, 21, 22]. The overall model presented in [15] takes into account numerous technological constraints, such as uplink and downlink minimal Signal-to-Interference Ratio (SIR), maximum emission power, antenna height constraints, antenna tilt and assumes a SIR-based power control mechanism.
- The UMTS technology standard is becoming obsolete with the deployment of Long Term Evolution (LTE) and 5G mobile telecommunication networks. Such modern networks, that offer higher connectivity rates, require installing new base stations. The question of the evolution from UMTS to LTE/5G networks [23] raised the interest of the academic community. This poses the question of the progressive deployment of these new technologies, in presence of the former ones: In [24] for instance, the authors consider a 5G deployment problem with some pre-existing base stations. The hardware to be deployed for these modern wireless networks is significantly different from classical UMTS antennas. One of the possible architecture for 5G networks is made of clusters, each of them consisting of a large number of small remote radio heads connected by optical fiber to a pool of baseband process units (BBU), which is wired to the uplink IP/MPLS network [23]. This architecture leads to dedicated optimization problems [25, 26, 27, 28]. Moreover, the operation of LTE/5G networks offers many flexibilities to maximize their efficiency. For example, some authors [29] propose a dynamic on/off switching of base stations for a better trade-off between energy consumption and quality of service. Such aspects could be taken into account in the deployment of a 5G network.
- The importance of the OWLD problem arises with the deployment of large-scale public and private WLANs, such as in airports, hotels or other buildings. This problem is related to the UMTS planning problem because (a) the location and the configuration of the Access Points (APs) may be optimized jointly and (b) interferences impact on the QoS. WLAN deployment, however, differs from UMTS planning in the following ways.
 - The configuration possibilities are more limited for WLAN deployment than UMTS.
 - The number of available frequencies is more limited for WLAN deployment [14]: this is why interference constraints are even more important.
 - The communication protocols used are different.
 - Indoor radio propagation is far more difficult to predict than outdoor and long-range propagation of GSM frequencies: in a building several physical effects, such as, e.g., reflections, diffractions, and self-interference, may impact the radio propagation. Hence, computing the electromagnetic field generated by an emitter in a building requires advanced simulators, based on the precise knowledge of the building's architecture. From this point of view, the OWLD problem is closer to the problem of deploying a 5G network, with a wavelength's order of magnitude around one millimeter, in an urban or indoor environment. Yet, it seems that most of the approaches found in the literature for optimal 5G deployments [24, 26, 28] still use simple empirical propagation models (see Sect. 1.2) that may not take into account the aforementioned physical effects.

The last point is a possible explanation as to why WLAN deployment problems have not been extensively studied from the point of view of OR/MP methods. Most of works devoted to optimize WLAN deployments appear to have been proposed by researchers in computer networking.

In this paper, we propose a global approach for the deployment of a WLAN network, which combines simulation and optimization. First, we provide a mathematical model for radio propagation in a building floor in order to perform accurate predictions via simulation. We overcome some remarkable theoretical and computational obstacles posed by the indoor environments, which possess a very high number of reflection and diffraction sources. The precision of the model and the corresponding simulation is critical for OWLD, since optimization using wrong input data would obviously yield wrong solutions. Based on the qualitative input data provided by the simulation tool, we then propose an optimization model for the OWLD problem, which brings together the most important features found in the literature.

1.2 | The state of the art on the OWLD problem

Many different approaches exist in order to streamline WLAN deployment processes in indoor space. In this subsection we try to summarize the main ingredients in optimizing WLAN deployments: decision variables, input data, optimization criteria, constraints, and algorithmic approaches.

1.2.1 | Decision variables

The decisions involved in deploying a WLAN are:

- AP positions, either from a continuous or discrete optimization point of view;
- AP antenna orientation;
- AP emission power;
- AP emission frequencies.

The simultaneous decision of AP placement and frequency assignment is discussed in the literature to some extent [30, 31, 32, 33]. Depending on the approach, the spatial network coverage may be given or subject to optimization.

1.2.2 | Simulating indoor radio-wave propagation

Optimizing any wireless network, and particularly a WLAN infrastructure in a building, requires a detailed knowledge of the way the electromagnetic waves propagate in the building, so as to predict the coverage area of each AP. Since there is an uncountable number of spatial point in a Euclidean space model of a building, it is obviously impossible to obtain such knowledge through empirical measurements. This is why it is necessary to have a reliable model to predict how electromagnetic waves propagate in a complex indoor environment. This step is crucial since it will be the input of the optimization problem. For more details, the strong impact of the Physical Layer (PHY) modeling on network performance prediction is illustrated in [34].

Next, we briefly discuss some relevant propagation models for WLAN signals in building floors consisting of rooms and aisles.

- *Empirical approaches.* These are based on statistical models of propagation [35, 36, 37]; they predict the average behavior of waves in typical environments, but fail to provide accurate predictions in each room of the WLAN coverage area. Such approaches are widely used in network design because of their low computational requirements. They model the path-loss L (in dB) between emitter e and receiver r , which is equivalent to the power gain ratio expressed in logarithmic scale: $L = 10 \log(\frac{P_e}{P_r})$, where P_e is the power emitted by e and P_r the power received by r , both expressed in watts (W).
 - One-slope model. The path-loss L (in dB) is simply a function of the distance d between transmitter and receiver antennas:

$$L(d) = L_0 + 10n \log(d),$$

where L_0 (in dB) is a reference loss value for a unit (1m) distance, n is a power decay factor, and d is a distance (expressed in m). L_0 and n are empirical parameters for a given environment, which fully control the prediction. In a barrier-free environment, theoretical values of L_0 and n can be determined for a given wavelength. In practice, there are always obstacles to signal propagation and there is then no other way to choose values for L_0 and n than calibration from measured data, using linear regression such that the difference between the measured and estimated path losses is minimized in a mean square error sense [38].

- Multi-wall model. A semi-empirical multi-wall model provides much better accuracy than the one-slope model, and the results are more site-specific. The path-loss L (in dB) is a function of the distance between transmitter and receiver antennas but also of simple architectural properties. We have

$$L(d) = L_0 + 10n \log(d) + \sum_{i=1}^N k_i L_i + \kappa_f \Lambda_f,$$

where k_i is the number of walls of type i (for i ranging over all considered wall types) between transmitter and receiver antennas, L_i (in dB) is the attenuation factor for the i -th wall type, N is the number of wall types, κ_f is the number of floors between transmitter and receiver, and Λ_f (in dB) is the floor attenuation factor. There are also no universal values for the parameters L_i and Λ_f , which have to be calibrated by means of a measurement campaign.

These models are easy to use and can produce their output quickly. However, their accuracy is limited. The loss of accuracy is mostly due to the lack of architecture details they take into account; specifically, they neglect the physical effects of diffraction, self-interference, and so on.

- *Geometrical optics based modelling.* Ray-tracing techniques are among the most popular methodologies for indoor radiowave propagation simulation [39, 40, 41, 42]. Ray-tracing simulations describe the physical wave propagation process, based on geometrical optics and the uniform geometrical theory of diffraction. Using Fermat's least time principle, a ray-tracing simulation determines a ray's trajectory between source point and some given field locations, which yields the propagation loss at these locations. Unlike empirical approaches, ray-tracing simulations take physical effects and indoor architecture into account, thus giving more precise results. Yet, their computational complexity is proportional to the number of rays *launched* by the source and grows exponentially with the number of reflections each ray undergoes. Therefore, the number of simulated reflections is usually limited. This leads to some undesirable effects due to the angular discretization. An attempt to decrease these effects, proposed by [41], consists in simulating "tubes" rather than "rays". Geometrical optic based methods are often presented in a three-dimensional (3D) setting; it turns out, however, that it is just as accurate, but more computationally efficient, to work with multiple two-dimensional (2D) simulations [43]. Most of the works in the field of geometrical optic based simulation are dedicated to the reduction of the computational complexity by designing efficient structures to represent the physical environment, so as to speed-up the computation of ray intersections [44, 45].
- *Finite differences modelling.* There exists a family of propagation models based on Maxwell's equations. The first indoor radio propagation simulations with finite differences were been proposed in [46, 47]. Another discrete approach, called "ParFlow", based on the cellular automaton formalism, and applied to urban micro-cellular GSM simulations, was proposed in [48]. The main advantage of such methods is to naturally model all propagation effects including reflection and diffraction. The price to pay is a high computational load, specially in a 3D setting. However, as explained in [49], such approaches appear to be well-suited to indoor environments since their computational complexity does not depend on the number of objects and reflections. Moreover, they can handle any shape of obstacle. In [49, 50, 51], the ParFlow theory is transposed to the frequency domain in order to compute steady-state propagation; the Multi-Resolution Frequency Domain ParFlow (MR-FDPF) algorithm allows the efficient solution of the associated linear system of equations. This method is presented either in a 2D or 3D setting; a so-called "2.5D" variant proposed in [50] enables the efficient simulation of radio propagation in multi-floor buildings. MR-FDPF was the first finite differences method capable of simulating electromagnetic fields in realistic buildings, with a prediction accuracy assessed by measurement campaigns [51].

1.2.3 | Deployment optimization criteria

There is a large variety of WLAN deployment quality evaluation functions in the literature. These functions are sometimes used as optimization criteria, and sometimes they are imposed as constraints to be satisfied.

- *Cost criteria.* A first optimization criterion for the deployment of a wireless network is naturally the economic cost, which mainly depends on the number of APs used and site-specific installation costs [53, 54].
- *Coverage criteria.* This family of criteria, which is very common in the literature on WLAN optimization, includes indicators that describe how well the network can cover the target area in terms of space and signal strength. One can mention the covered surface criterion or the numbers of covered clients [56]. The "hard cover" constraint refers to the fact that each client must receive a signal with an intensity higher than a given threshold [30, 53, 54, 57, 58]. An optimization objective used in [57, 59] is the sum of power received by each client from the best AP server, whereas authors in [56, 59] use the min - max criterion of received power from the best server at the worse client location.
- *Interference and Quality of Service criteria.* Another family of criteria focuses on the QoS for the clients rather than the absolute strength of the received signal. The QoS mainly depends on the signal strength but also on the interference sources, this is why the SIR or the Signal Interference-plus-Noise Ratio (SINR) are often used. These criteria are either involved as a hard QoS constraint to enable data rate guarantee for every or are used as an aggregated criteria (average). Some articles distinguish uplink and downlink SIR [53, 54, 58]. Another QoS metric is the Maximum of Channel Utilization, which designates the maximum traffic loads assigned to an AP. This is a practical metric for the wireless network performance, because it explains qualitatively its congestion [30]. More sophisticated approaches use simulation tools to compute QoS metrics depending on the selected networking protocol [60].
- *Client positioning accuracy criterion.* In some cases, a deployment criterion may be the ability of the system to locate client devices by a triangulation process based on Wi-Fi communication protocol [61].
- *Multiobjective approach and aggregate criteria.* Some authors are interested in finding deployment solutions with balanced characteristics between different criteria among those mentioned above. In [62], a multiobjective approach is implemented to obtain such a balanced solution. Other approaches use aggregated criteria, which often are a linear combination of some of the above-mentioned criteria [56, 59, 60]. The weights before each criterion are often chosen heuristically.

1.2.4 | Solution methods

The diversity of criteria yields a corresponding diversity of discrete, continuous, convex, and non-convex problems, as well as solution methods. Some approaches use Binary Linear Programming (BLP) or Mixed Integer Linear Programming (MILP) formulations and employ standard branch-and-bound solvers [30, 53, 57], or propose dedicated Dantzig-Wolfe decompositions [63]. Other approaches use convex optimization techniques, such as the Simplex Algorithm [59], the Bundle Methods [56], the Nelder-Mead Algorithm [56], the Quasi-Newton BFGS Algorithm and the conjugate gradient search procedure [59, 64]. A wide range of metaheuristics are also used in the literature of WLAN deployment optimization: genetic algorithms [56, 59, 65], Simulated Annealing [59], Large-Neighbourhood and Tabu Searches [54], Termite Colony Algorithm [55] or Particle Swarm Optimization [66, 67]. Finally, a few authors use techniques from Constraint Programming [58, 68] and Black-Box Optimization [60, 69].

1.3 | Positioning in relation with the state of the art

In this paper we propose an integrated approach in two phases: in the first phase we estimate the force of the magnetic field generate by a source in the building floor by solving the Helmholtz differential equations. In the second phase we formulate the OWLD optimization problem using input from the first phase, and we solve it using a number of exact and heuristic techniques based on MP. The approaches found in the literature to address the OWLD differ in either the first or the second phase or both. An integrated approach was never proposed so far to the best of our knowledge.

1.3.1 | Simulation methodology

The main goal of the project that motivated this paper was to find a site-specific procedure that could take into account the shape of the building hosting the wireless network. We were looking for a simulation methodology more realistic than an empirical model; we were interested in approaches based on Maxwell's equations [46, 47, 48, 49, 50, 51] because they appeared to be the canonical point of view in physics. They took into account the physical effects of interest, i.e. *reflections, diffraction, self-interference or corridor effect*. The alternative point of view, provided by geometrical optics, appeared more complicated to implement. Inspired by the MR-FDPF method [49, 50, 51], we also chose to work in the Fourier domain in order to obtain a partial differential equation (PDE) without time dependence and with uncoupled frequencies: the Helmholtz equation. We therefore solved this PDE using simple finite difference schema by a state-of-the-art sparse linear solving library [70]. This way, we obtained a similar time complexity as the MR-FDPF method, with an easier implementation.

1.3.2 | Modelling the deployment problem

In this section we list the techniques on which our methodology is based:

- We use Binary Linear Programming as in [30, 53, 57] to model the overall decision problem, which employes elements from facility location, frequency assignment and knapsack.
- We optimize jointly over client positions, AP positions and channel assignment.
 - Clients: we consider a certain number of given positions to place clients at. In the case of a corporate building for instance, these positions would correspond to workstations for employees, needing a WiFi connection. Each client requires a certain uploading and downloading data rate. For linear modelling purposes, we consider only two possible alternatives for a client: it is either connected and receives the demanded data rates or is disconnected.
 - Access points placement: we consider also a list of predetermined available locations to place APs. A specific cost corresponds to each of these locations, describing the installation and maintenance costs. We consider APs of only one type. We chose not to consider repeaters, which are rarely used in large-scale deployment project due to their lack of reliability.
 - Available channels and interference: we consider a set \mathcal{C} of available communication channels (i.e. frequencies) at our disposal for the WiFi network deployment. The IEEE 802.11 WLAN standard defines a fixed number of channels for use by APs and mobile users. [A total of 13 frequencies is available in the 2.4GHz range but these channels may be overlapping if the used bandwidth is large. In practice, only 3 frequencies are often used in the same physical neighborhood simultaneously \[14\]. Therefore, we considered here cases with three available non-interfering channels: \$|\mathcal{C}| = 3\$. We also considered cases with 6 available channels, since one could also simultaneously use channels in the 5GHz range.](#)
- Abandonment of the APs orientation variables: after exchanging with network experts [52], we thought it was not realistic to optimize in such a level of detail because [the antennas orientation of WLAN routers has a negligible impact](#) compared to unpredictable perturbation sources such as moving obstacles.

- Presence of extra noise: our model involves an ambient noise that represents the thermal noise and the presence of perturbation sources from the surrounding environment. Taking into account ambient noise leads to more robust solutions.
- Impact of the interference and of the noise on the QoS: it is well known that the interference between devices impacts the data communication rate. We use the Shannon-Hartley theorem to express channel capacity as a function of noise and interference levels as in [53, 54, 58], for uplink and downlink connections. The theoretical capacity of a wireless channel is given by Shannon's law:

$$C = B \log_2 \left(1 + \frac{S}{N} \right) \quad (1)$$

where B is the available bandwidth in Hz (Hertz), S the signal strength and N the interference-plus-noise level in W (Watts). For fixed bandwidth \bar{B} and signal strength values \bar{C} and \bar{S} , the maximal interference-plus-noise level compatible with data rate \bar{C} is thus:

$$N_{\max}(\bar{C}, \bar{B}, \bar{S}) = \frac{\bar{S}}{2^{\bar{C}/\bar{B}} - 1}. \quad (2)$$

The presence of an ambient noise implies that any connection in our deployment will comply not only with a minimum SINR ratio but also with a minimum signal strength in absolute value.

- Communication protocol: an important modeling issue is the role of the communication protocol, which greatly impacts the data communication rate in practice. In particular, the main issue is the interaction of multiple client devices connected to a same AP. In this article, we refer to the Carrier Sense Multiple Access with Collision Avoidance (CSMA/CA) method used in the IEEE 802.11 standard, which is the most common WLAN protocol [71]. The CSMA/CA method uses a collision avoidance mechanism based on a principle of prior negotiation and reciprocal acknowledgements between sender and receiver. The station wishing to transmit listens to the network. If the network is busy, the transmission is delayed. Otherwise, if the media is free for a given time then the station can transmit. No two clients may emit at the same time. Hence, we can assume that clients connected to the same AP do not interfere. We denote the set of any AP and its connected clients as *cluster*. Inside a cluster, every device is tuned to the same channel. The maximal data rate implied by CSMA/CA mode for each cluster will be taken into account as a capacity γ for each AP. Two clusters tuned to different channels are assumed not to interfere with each other. By contrast, two clusters tuned to the same channel do interfere: more explicitly, in Shannon's law Eq. (1) the variable N is a sum of a ambient noise θ and of all signals received from other clusters on the same channel, i.e. all the interfering signals.
- Economic objective: we study the trade-off between installation and maintenance costs, and the total data-rate that the infrastructure can provide, as in the UMTS network planning problem presented in [15]. We penalize each data-flow unit that is requested by a client but not provided by the network as deployed, at a cost ρ .

1.4 | Outline of the article

The rest of this article is organized as follows: Section 2 presents our methodology for simulating the propagation of electromagnetic waves in an indoor environment, which is based on a finite-difference scheme of the Helmholtz PDE; Section 3 introduces a BLP formulation for the OWLD problem based on the output from the simulator, and another BLP formulation for a natural relaxation of OWLD problem; Section 4 states that the OWLD problem and its relaxation are both strongly NP-hard; Section 5 proposes heuristic algorithms to try to find better solutions in case an exact algorithm would fail to close the optimality gap; Finally, Section 6 presents our numerical experiments and the results obtained.

2 | SOLVING THE HELMHOLTZ EQUATION

In this section, we introduce a numerical methodology used to predict radio propagation in any building whose shape and materials are known precisely, as detailed below. Our approach is freely inspired by the MR-FDPF method of Gorce et al. [49, 50, 51] but it leads to an easier implementation based on the sparse linear algebra library SuperLU [70]. It is a simple finite difference schema to simulate Helmholtz equation, a PDE defined on complex numbers which is the transposition of the classic wave equation in frequency domain.

2.1 | Why the Helmholtz equation?

2.1.1 | The classical wave equation

Following the same modelling simplifications from [48] and [72], for instance, we consider a 2D environment and a transverse electromagnetic field, enabling us to model it as scalar wave. We start from the following classical two-dimensional wave equation in an heterogeneous medium:

$$\Delta u(x, y, t) - \mu \epsilon \partial_t^2 u(x, y, t) = -s(x, y, t) \quad (3)$$

where $u(x, y, t)$ is the unknown real-valued function representing the scalar wave, $s(x, y, t)$ is a source term, $\epsilon(x, y)$ is the local electric permittivity and $\mu(x, y)$ the local permeability. The physical values ϵ and μ depend on the material: they represent the architecture of the floor.

2.1.2 | The frequency domain

In order to eliminate the time differential, the Fourier transform is applied to the wave equation (3), which gives the Helmholtz equation:

$$\Delta \Psi(x, y, \omega) + \omega^2 \mu \epsilon \Psi(x, y, \omega) = -S(x, y, \omega) \quad (4)$$

where Ψ is the Fourier transform of u and S is the Fourier transform of s . The main advantage of this wave equation in the frequency domain is the absence of partial derivative with respect to (w.r.t.) ω , the angular frequency variable: every frequency can be studied independently, leading to the case of one single harmonic source. In the following, we assume that the source signal is only made of its carrier frequency f_c , which corresponds to the angular frequency $\omega_c = 2\pi f_c$. The Helmholtz equation can thus be written:

$$\Delta \Psi(x, y) + \omega_c^2 \mu \epsilon \Psi(x, y) = -S(x, y, \omega_c). \quad (5)$$

The scalar field Ψ represents the intensity of the electromagnetic field in the steady state corresponding to frequency f_c . In such a steady state there is no propagation anymore. We let c_0 denote the light speed in vacuum and $\lambda_c = \frac{c_0}{f_c}$ denotes the carrier wavelength.

2.2 | Boundary conditions and the additional diffusive term

2.2.1 | Boundary conditions

In any PDE, it is crucial to set the boundary conditions of the equation in order to define the problem exactly. Here we impose a Dirichlet condition: the definition domain is a rectangle $[0, L] \times [0, \ell]$ and Ψ has to be null on the boundary. However, setting a null field value on the boundary creates fictitious reflections in the simulation. Indeed this Dirichlet condition corresponds to a situation where the boundary is a perfectly reflecting material: no outgoing energy transfer.

2.2.2 | Avoiding spurious reflections

In preliminary simulations, fictitious patterns of interference were observed: the reflections on the walls and on the boundary were overestimated. A solution employed in [50] consists in adding a diffusive term in the boundary, in the walls. This diffusive term models walls energy absorption and the energy transfer to the outside. Helmholtz equation (5) can now be written:

$$\Delta \Psi(x, y) + \mu(x, y) (\omega_c^2 \epsilon(x, y) - i\omega_c \sigma(x, y)) \Psi(x, y) = -S(x, y, \omega_c) \quad (6)$$

where $\sigma(x, y)$ is a fictive electric conductivity that is strictly positive in the walls and in the boundary (see Assumption 1). The complex two-dimensional equation (6) is the ultimate PDE that we simulate.

2.3 | Finite difference approach

2.3.1 | Discretization

The rectangle $[0, L] \times [0, \ell]$ is discretized into a grid $\{0, \dots, N_x - 1\} \times \{0, \dots, N_y - 1\}$, using the same step $h > 0$ for both dimensions. We let d denote the integer $N_x N_y$ and index the grid by the set $\{0, \dots, d - 1\}$. We assume that $N_x \geq 3$. We will discretize the field Ψ so that, for any $(p, q) \in \{0, \dots, N_x - 1\} \times \{0, \dots, N_y - 1\}$ the scalar $\Psi_{j_{N_x+i}}$ is an approximation of $\Psi(hp, hq)$. We define $\mathcal{G} = (\{0, \dots, d - 1\}, \mathcal{E})$ the unoriented graph associated to grid $\{0, \dots, N_x - 1\} \times \{0, \dots, N_y - 1\}$. The classic discretization of Laplacian operator in (6) leads to the following equation:

$$\sum_{\substack{l=0, \dots, d-1 \\ \{k, l\} \in \mathcal{E}}} \Psi_l + (\beta^2 n_k^2 - 4 - ih^2 \omega_c \alpha_k) \Psi_k = F_k, \quad \forall k \in \{0, \dots, d - 1\} \quad (7)$$

with the following conventions:

- normalization constant: $\beta = \frac{\omega_c h}{c_0}$
- diffusive term: $\alpha_{qN_x+p} = \mu(\text{hp}, \text{hq}) \sigma(\text{hp}, \text{hq}), \forall (\text{p}, \text{q}) \in \{0, \dots, N_x - 1\} \times \{0, \dots, N_y - 1\}$
- refractive index: $n_{qN_x+p} = c_0 \sqrt{\mu(\text{hp}, \text{hq}) \epsilon(\text{hp}, \text{hq})}, \forall (\text{p}, \text{q}) \in \{0, \dots, N_x - 1\} \times \{0, \dots, N_y - 1\}$
- source term: $F_{qN_x+p} = -h^2 S(\text{hp}, \text{hq}, \omega), \forall (\text{p}, \text{q}) \in \{0, \dots, N_x - 1\} \times \{0, \dots, N_y - 1\}$.

We define the matrix $U \in \mathbb{R}^{d \times d}$ as the adjacency matrix associated to the grid graph \mathcal{G} and let $L = 4I_d - U$, where I_d is the $d \times d$ identity matrix. We also define the diagonal matrix $D \in \mathbb{R}^{d \times d}$ associated to vector $(\beta^2 n_k^2 - ih^2 \omega_c \alpha_k)_{0 \leq k \leq d-1}$. Defining also $A = D - L \in \mathbb{R}^{d \times d}$, the problem to be solved can be cast as following linear system

$$A\Psi = F, \quad \Psi \in \mathbb{R}^d. \quad (8)$$

Broadly speaking, the A matrix represents the architecture of the building while F represents the intensities and source positions. In the application cases we present here, we have to calculate the electromagnetic field produced from each source points, whose set is designated by $V \subset \{0, \dots, d-1\}$. For each source point $i \in V$ we need to solve a linear system with the same system matrix A but with specific right-hand side (RHS) member $F^i = P_i e_i \in \mathbb{R}^d$ where $P_i \in \mathbb{R}$ is the power of device i and $e_i \in \mathbb{R}^d$ is the canonical basis vector associated to i . In practice, P_i has only two possible values in our experiments, depending on whether i is a client device (P_{client}) or a candidate point to host an AP (P_{AP}). The electromagnetic field generated by $i \in V$ is the solution of linear system (8) with $F = F^i$; this solution is denoted Ψ^i . For any $(i, j) \in V \times V$, the power $p_{ij} \in \mathbb{R}_+$ received by j from emitter i is:

$$p_{ij} = |\Psi_j^i| \quad (9)$$

where Ψ^i is the solution of (8) associated to F^i . The matrix $p = (p_{ij})$ provides the input to the optimization problem introduced in Sect. 3. Before proving the invertibility of the system to be solved, we make a modeling assumption. This numerical condition avoids spurious reflections (see Sect. 2.2) and is useful to prove the invertibility.

Assumption 1. For any cell (p, q) such that $p \in \{0, 1, N_x - 2, N_x - 1\}$ or $q \in \{0, 1, N_y - 2, N_y - 1\}$, we have $\alpha_{qN_x+p} > 0$.

Proposition 1. Under Assumption 1, the system matrix A is invertible.

Proof. We take any complex vector $\Psi \in \mathbb{C}^d$ such that $A\Psi = 0$, and we are going to prove that $\Psi = 0$. This will prove the proposition since A is a square matrix.

1. First, we prove that for any $k \in \{0, \dots, d-1\}$ such that $\alpha_k > 0$, we have $\Psi_k = 0$. Decomposing matrix $D = R - iJ$, where R is the diagonal matrix associated to vector $(\beta^2 n_k^2)_{0 \leq k \leq d-1}$ and J the diagonal matrix associated to vector $(h^2 \omega_c \alpha_k)_{0 \leq k \leq d-1}$, matrix A can be written as $A = R - iJ - L$. Since $A\Psi = 0$, the following holds

$$\Psi^* R \Psi - i(\Psi^* J \Psi) - \Psi^* L \Psi = 0 \quad (10)$$

Since matrices R , J , and L are real symmetric matrices, we know that $(\Psi^* R \Psi, \Psi^* J \Psi, \Psi^* L \Psi) \in \mathbb{R}^3$. Hence, we can deduce from (10) that $\Psi^* J \Psi = 0$, by unicity of the imaginary part. Reformulating this, we have that $h^2 \omega_c \sum_{k=0}^{d-1} \alpha_k |\Psi_k|^2 = 0$. Dividing by $h^2 \omega_c > 0$, we have $\sum_{k=0}^{d-1} \alpha_k |\Psi_k|^2 = 0$. Since $\alpha_k |\Psi_k|^2 \geq 0$ for all $k \in \{0, \dots, d-1\}$, we deduce that $\alpha_k |\Psi_k|^2 = 0$ and thus $(\alpha_k > 0) \implies (\Psi_k = 0)$.

2. Based on this first point and using Assumption 1, we deduce that $\Psi_{qN_x+p} = 0$ for all (p, q) such that $p \in \{0, 1, N_x - 2, N_x - 1\}$ or $q \in \{0, 1, N_y - 2, N_y - 1\}$. This means that field vector Ψ is null in the proximity of boundaries.
3. We are now going to prove by finite strong induction over $k \in \{0, 1, \dots, d-1\}$ that $\Psi_k = 0$.

- Initialization: in the second argumentation point above, we proved that $\Psi_0 = 0$.
- Induction step: we take $k \in \{0, \dots, d-2\}$ and we assume that $\Psi_l = 0$ for all $l \in \{0, \dots, k\}$. We decompose k as $qN_x + p$. In a first case, we have that $p \in \{0, 1, N_x - 2, N_x - 1\}$ or $q \in \{0, 1, N_y - 2, N_y - 1\}$, and thus $\Psi_k = 0$ (see second argumentation point). In a second case, we have that $(p, q) \in \{2, \dots, N_x - 3\} \times \{2, \dots, N_y - 3\}$. We apply then the system equation (7) with a null RHS member and for index $\tilde{k} = k + 1 - N_x$, which gives

$$\Psi_{k+2-N_x} + \Psi_{k-N_x} + \Psi_{k+1} + \Psi_{k+1-2N_x} + (\beta^2 n_k^2 - 4 - ih^2 \omega_c \alpha_k) \Psi_{k+1-N_x} = 0. \quad (11)$$

We recall that $N_x \geq 3$ by assumption, thus the integers $k+2-N_x, k-N_x, k+1-2N_x, k+1-N_x$ are less than or equal to k . Using the strong induction hypothesis, we know that $\Psi_{k+2-N_x} = \Psi_{k-N_x} = \Psi_{k+1-2N_x} = \Psi_{k+1-N_x} = 0$. Hence, equation (11) gives that $\Psi_{k+1} = 0$.

By strong induction, we proved that $\Psi_k = 0$ for all $k = 0, \dots, d - 1$.

□

2.3.2 | Solution algorithm and time complexity

We need to solve $|V|$ linear systems sharing the same matrix $A \in \mathbb{R}^{d \times d}$ but corresponding to different RHS member $F \in \mathbb{R}^d$. Hence, it is worth computing the LU factorization of this matrix as a first step in order to speed up the solution time of every single linear system thereafter, see the next paragraph for the complexity details. One can benefit from the non-zero structure of the entries of A by ordering the eliminations such that as few non-zeros as possible are generated in L and U , because the number of non-zeros determines the storage and time complexities of the triangular solves [73, 74]. For a 2-D regular grid like matrix A , we need $O(d^{\frac{3}{2}})$ floating point operations for a sparse factorization, and the L,U factors one obtains have $O(d \log d)$ non-zeros, see [75, 76]. Hence, based on the LU decomposition, a system is solved in $O(d \log d)$ floating point operations. Considering that $N_x \geq N_y$, the time complexity of the two algorithmic steps are thus the following:

- $O(N_x^3)$ for the LU factorization of the system
- $O(N_x^2 \log N_x)$ to compute the system solution based on the LU factorization.

Since we want to compute the electromagnetic field generated by $|V|$ different sources, we can see that the preliminar factorization enables to achieve it in $O(N_x^3 + |V|N_x^2 \log N_x)$ instead of $O(|V|N_x^3)$. The resulting time complexity is similar to the complexity of 2D MR-FDPF claimed in [49] but our approach lead to a more direct implementation by using a state-of-the-art linear algebra library.

2.4 | The “2.5-th” dimension

To make the model fit reality, it is crucial to model indoor radio wave propagation in 3D environment. Transposing this finite-difference method in 3D would yield an excessive increase of the time required to solve the systems. Instead, we consider the 2.5D empirical approach presented in [50], which relies on the projections of the field in the floor $k - 1$ and $k + 1$ to compute the field in the floor k , using one of these alternatives:

- *Field Projecting* models the 3D propagation by projecting the field map (of the floor $k - 1$ and $k + 1$) through the ceilings with an attenuation coefficient depending on the nature of the ceilings.
- *Source Projecting* consists in projecting the sources (on floors $k - 1$ and $k + 1$) in floor k with an attenuation factor and then in computing the 2D propagation in floor k from this virtual source.
- A linear combination thereof.

3 | OPTIMAL WLAN DEPLOYMENT: MP FORMULATIONS

In this section, we introduce a new WLAN deployment optimization problem that addresses many of the challenges that we found in the literature. We also introduce a simple relaxation of this deployment problem and we prove that both the problem and this relaxation are strongly NP-hard. Finally, we introduce in this section several solution algorithms.

3.1 | Binary linear programming formulation

We denote by (P) the BLP formulation introduced in this subsection. This is the OWLD problem.

Sets of points

We consider subsets of a 2D or 3D simulation grid:

- I defines the set of users (clients) to be covered.
- J defines the set of eligible positions for APs. A point which has to be covered and which is also a potential AP position is duplicated. We can therefore assume that $I \cap J = \emptyset$.
- $V = I \cup J$.

Set of channels

\mathcal{C} denotes the set of available frequencies.

Parameters

Table 1 introduces the parameters involved in our BLP formulation. We make two assumptions: (a) the data flows u_i and d_i are scaled by the available bandwidth, which is known to be the same for every channel; (b) the different channel carrier frequencies are distinct enough not to interfere, but close enough to assume that the signal strength p_{ij} does not depend on the channel. These assumptions are satisfied for any deployment in the IEEE 802.11 protocol with sufficiently separated channels [14]. Moreover, the fact that the signal strength does not significantly depend on the channel can be numerically checked with the simulation tool. Finally the last parameter of this optimization problem is a "big-M" constant defined as $M = \theta + \sum_{(i,j) \in \mathcal{V}^2} p_{ij}$.

Notation	Index set	Meaning
$p_{ij} \in \mathbb{R}_+$	$\mathcal{V} \times \mathcal{V}$	Signal emitted by i and received by j computed with methodology presented in Sect. 2
$c_j \in \mathbb{R}_+$	\mathcal{J}	AP installation cost at position j
$u_i \in \mathbb{R}_+$	\mathcal{I}	Data flow (normalised by the bandwidth) client i wants to upload
$d_i \in \mathbb{R}_+$	\mathcal{I}	Data flow (normalised by the bandwidth) client i wants to download
$K_{ij}^u \in \mathbb{R}_+$	$\mathcal{I} \times \mathcal{J}$	Maximal interference-plus-noise level at i for uplink connection between client i and AP j
$K_{ij}^d \in \mathbb{R}_+$	$\mathcal{I} \times \mathcal{J}$	Maximal interference-plus-noise level at j for downlink connection between client i and AP j
$\gamma \in \mathbb{R}_+$		Flow capacity of any AP
$\theta \in \mathbb{R}_+$		Ambient noise level
$\rho \in \mathbb{R}_+$		Marginal penalty cost for non-provided flow unit

TABLE 1 Parameters

Set of edges

Given an ambient noise level $\theta > 0$, the set

$$E_\theta = \{(i, j) \in \mathcal{I} \times \mathcal{J} \mid (\theta \leq K_{ij}^u) \wedge (\theta \leq K_{ij}^d)\}$$

is the set of potential wireless connections, i.e. the set of all the user-AP pairs such that the signal strength is strong enough to enable uplink and downlink flow in spite of the ambient noise. We actually consider the undirected graph induced by $G = (\mathcal{V}, E_\theta)$, which we denote in the same way with a slight abuse of notation. This undirected graph is bipartite.

Decision variables

Table 2 introduces the decision variables of our BLP formulation. Having $x_i = 1$ means that device i is on, $w_{ic} = 1$ means that device i is tuned on channel c and $y_{ij}^c = 1$ describes that client i is served by the AP j on channel c . In this BLP problem, the total number of decision variables is $(1 + |\mathcal{C}|) \times |\mathcal{V}| + |\mathcal{C}| \times |E_\theta|$.

Notation	Index set	Meaning
$x_i \in \{0, 1\}$	\mathcal{V}	Device i is on/off
$w_{ic} \in \{0, 1\}$	$\mathcal{V} \times \mathcal{C}$	Device i emits on channel c
$y_{ij}^c \in \{0, 1\}$	$E_\theta \times \mathcal{C}$	Client i communicates with AP j on channel c

TABLE 2 Decision variables

Objective

Minimize the sum of the device installation costs, and the cost for not covering some of the clients:

$$\sum_{j \in J} c_j x_j + \rho \sum_{i \in I} (d_i + u_i)(1 - x_i). \quad (12)$$

Constraints

One coupling constraint:

- Each device is tuned to a unique channel:

$$\sum_{c \in \mathcal{C}} w_{ic} = x_i, \quad \forall i \in V \quad (13)$$

The other constraints are channel dependant (uncoupled):

- Each client communicates with one AP:

$$\sum_{\substack{j \in J \\ (i,j) \in E_\theta}} y_{ij}^c = w_{ic}, \quad \forall c \in \mathcal{C}, \forall i \in I \quad (14)$$

- Maximal capacity of an AP:

$$\sum_{\substack{i \in I \\ (i,j) \in E_\theta}} (d_i + u_i) y_{ij}^c \leq \gamma w_{jc}, \quad \forall c \in \mathcal{C}, \forall j \in J \quad (15)$$

- A client can communicate with an AP only if both are tuned to the same channel:

$$y_{ij}^c \leq w_{ic}, \quad \forall c \in \mathcal{C}, \forall (i,j) \in E_\theta \quad (16)$$

$$y_{ij}^c \leq w_{jc}, \quad \forall c \in \mathcal{C}, \forall (i,j) \in E_\theta \quad (17)$$

- Interference-plus-noise constraints at clients, to enable downlink flow:

$$\theta + \sum_{\substack{k \in I \\ k \neq i}} p_{ki} (w_{kc} - y_{kj}^c) + \sum_{\substack{k \in J \\ k \neq j}} p_{ki} w_{kc} \leq K_{ij}^d + M(1 - y_{ij}^c), \quad \forall c \in \mathcal{C}, \forall (i,j) \in E_\theta \quad (18)$$

- Interference-plus-noise constraints at candidates, to enable uplink flow:

$$\theta + \sum_{\substack{k \in I \\ k \neq i}} p_{kj} (w_{kc} - y_{kj}^c) + \sum_{\substack{k \in J \\ k \neq j}} p_{kj} w_{kc} \leq K_{ij}^u + M(1 - y_{ij}^c), \quad \forall c \in \mathcal{C}, \forall (i,j) \in E_\theta. \quad (19)$$

Constraint (18) enables to certify that, if $y_{ij}^c = 1$ i.e. if client i is connected to AP j on channel c , the sum of the ambient noise and the interference from other clusters tuned on the same channel will not exceed the maximal bearable level K_{ij}^d . On the contrary if $y_{ij}^c = 0$, this constraint is necessarily satisfied by definition of constant M . Constraint (19) is similar to [Constraint \(18\)](#) but looking at the maximal interference-plus-noise level at APs so as to make the uplink flows possible.

3.2 | Relaxing the interference-plus-noise constraints

In the case where the number of available channels is large (i.e. greater than the number of deployed APs), there is no interference problem between "clusters" anymore since each used channel is assigned to a unique AP. In such a case one can model the problem with less variables. We let (R) be the relaxation of (P) obtained by removing the channel bound constraints.

Decision variables

Table 3 introduces the decision variables of this relaxed problem.

Notation	Index set	Meaning
$x_i \in \{0, 1\}$	V	Device i is on/off
$y_{ij} \in \{0, 1\}$	E_θ	Client i communicates with AP j

TABLE 3 Decision variables

Objective

Minimize the sum of the installation and penalty cost:

$$\sum_{j \in J} c_j x_j + \rho \sum_{i \in I} (d_i + u_i)(1 - x_i).$$

Constraints

- Each client communicates with one AP:

$$\sum_{\substack{j \in J \\ (i,j) \in E_\theta}} y_{ij} = x_i, \quad \forall i \in I \quad (20)$$

- Maximal capacity of an AP:

$$\sum_{\substack{i \in I \\ (i,j) \in E_\theta}} (d_i + u_i) y_{ij} \leq \gamma x_j, \quad \forall j \in J \quad (21)$$

- A client can communicate with an AP only if both are on:

$$y_{ij} \leq x_i, \quad \forall (i,j) \in E_\theta \quad (22)$$

$$y_{ij} \leq x_j, \quad \forall (i,j) \in E_\theta. \quad (23)$$

We underline that the problem (R) depends on signal strength data computed with the simulator and on the parameters K_{ij}^u, K_{ij}^d through the definition of the set of edges E_θ . This relaxation has the advantage of providing a better lower bound than the continuous relaxation. Admittedly, we will show in the Sect. 4 that this optimization problem is NP-hard, but in practice it is easier to solve than the initial problem. Hence, we use this relaxation to build heuristic algorithms, see Sect. 5.

4 | COMPLEXITY RESULTS

4.1 | Complexity of the interference-free relaxation

Proposition 2. The decision problem associated with (R) is strongly NP-complete.

Proof. Table 4 introduces (R_D) , the decision problem associated with (R), whereas Table 5 introduces the classic (BinPacking) problem, which is known to be strongly NP-complete [77]. We now show a polynomial reduction of (BinPacking) to problem (R_D) , which prove the proposition

Problem:	(R_D)
Instance:	Sets I, J Rational numbers $p_{ij}, c_j, u_i, d_i, K_{ij}^u, K_{ij}^d, \gamma, \theta, \rho$ as detailed in Table 1 Rational number Q
Question:	Does there exist a feasible solution of (R) with cost less than or equal to Q ?

TABLE 4 Decision problem (R_D)

since (R_D) , as a BLP feasibility problem, is in NP. For any instance $\mathcal{I} = (N, K, s_1, \dots, s_N, L)$ of (BinPacking), we define an instance $\Phi(\mathcal{I})$ of (R_D) as:

Problem:	(BinPacking)
Instance:	Positive integers N, K with $K \leq N$ Positive integers s_1, \dots, s_N, L
Question:	Can we pack N objects of size s_1, \dots, s_N in K boxes of capacity L ?

TABLE 5 Decision problem (BinPacking)

- Sets: $I = \{1, \dots, N\}$ (clients), $J = \{N + 1, \dots, N + K\}$ (APs), $V = I \cup J$
- Parameters:
 - $p_{ij} = 1, \forall (i, j) \in V^2$
 - $c_j = 0, \forall j \in J$
 - $u_i = d_i = \frac{s_i}{2}, \forall i \in I$
 - $K_{ij}^u = K_{ij}^d = 1, \forall (i, j) \in I \times J$
 - $\gamma = L$
 - $\theta = 0$
 - $\rho = 1$

In such an instance, the graph G_θ is the complete bipartite graph associated to sets I and J .

- Level parameter $Q = 0$

With such a definition, it is clear that \mathcal{I} is a YES instance of (BinPacking) if and only if $\Phi(\mathcal{I})$ is a YES instance of (R_D) :

- If \mathcal{I} is a YES instance of (BinPacking), we can define the binaries y_{ij} associated to the presence of object i in box j . We also define $x_i = 1$ for all $i \in V$. Since $\sum_{i \in I} s_i y_{ij} \leq L$ for all $j \in J$, we have $\sum_{i \in I} (u_i + d_i) y_{ij} \leq \gamma x_j$ for all $j \in J$. Hence, (\mathbf{x}, \mathbf{y}) is a feasible solution of problem (R) associated to parameters of instance $\Phi(\mathcal{I})$, and has an objective value equal to $0 \leq Q$. This is why (\mathbf{x}, \mathbf{y}) certifies that $\Phi(\mathcal{I})$ is a YES instance of (R_D) .
- If $\Phi(\mathcal{I})$ is a YES instance of (R_D) , it exists (\mathbf{x}, \mathbf{y}) feasible in (R_D) and with value equal to zero. This means, in particular, that
 - $x_i = 1$ and $\sum_{j \in J} y_{ij} = 1$ for all $i \in I$
 - $\sum_{i \in I} (u_i + d_i) y_{ij} = \sum_{i \in I} s_i y_{ij} \leq L x_j$ for all $j \in J$

Thus, the vector \mathbf{y} is an explicit allocation of N objects of size s_1, \dots, s_N in K boxes of capacity L , and certifies that \mathcal{I} is a YES instance of (BinPacking).

Moreover, $\Phi(\mathcal{I})$ is computable with a time complexity polynomial in N and, thus, polynomial in the coding size of \mathcal{I} , since $N \leq |\mathcal{I}|$. \square

4.2 | Complexity of the OWLD problem

From the previous complexity result, the complexity of the OWLD problem can now be addressed.

Corollary 1. The decision problem associated with (P) is strongly NP-complete.

Proof. Table 6 introduces (P_D) , the decision problem associated with (P) . We are going to show a polynomial reduction of (R_D) to problem (P_D) , which will prove the proposition since (P_D) , as a BLP feasibility problem, is in NP.

For any instance $\mathcal{I} = (I, J, p_{ij}, c_j, u_i, d_i, K_{ij}^u, K_{ij}^d, \gamma, \theta, \rho, Q)$ of (R_D) , we define an instance $\Psi(\mathcal{I})$ of (P_D) with same coefficients and $\mathcal{C} = J$. With such a definition, it is clear that \mathcal{I} is a YES instance of (R_D) if and only if $\Psi(\mathcal{I})$ is a YES instance of (P_D) :

- If \mathcal{I} is a YES instance of (R_D) , it exists a solution $(\mathbf{x}, \mathbf{y}) \in \{0, 1\}^V \times \{0, 1\}^{E_\theta}$ feasible for this instance of problem (R_D) and with value less than or equal to Q . In order to construct a feasible solution of (P) , each cluster will be assigned its own channel. Formally, we define the binary vectors $\tilde{\mathbf{y}} \in \{0, 1\}^{E_\theta \times \mathcal{C}}$ and $\mathbf{w} \in \{0, 1\}^{V \times \mathcal{C}}$ as follow:

Problem:	(P _D)
Instance:	Sets I, J, C Rational numbers p _{ij} , c _j , u _i , d _i , K _{ij} ^u , K _{ij} ^d , γ, θ, ρ as detailed in Table 1 Rational number Q
Question:	Does there exist a feasible solution of (P) with cost less than or equal to Q?

TABLE 6 Decision problem (P_D)

- $\tilde{y}_{ij}^c = y_{ij} \delta_{jc}$ for all $(i, j) \in E_\theta$ and $c \in C$, where δ_{jc} denotes the Kronecker product between j and c
- $w_{ic} = x_i \delta_{ic}$ for all $i \in J$ and $c \in C$
- $w_{ic} = \sum_{\substack{j \in V \\ (i,j) \in E_\theta}} \tilde{y}_{ij}^c$ for all $i \in I$ and $c \in C$.

By construction (x, \tilde{y}, w) is feasible for the instance $\Phi(\mathcal{I})$ of problem (P) and has value $\sum_{j \in J} c_j x_j + \rho \sum_{i \in I} (d_i + u_i)(1 - x_i)$ which is lower or equal to Q by definition of (x, y) . It certifies that $\Phi(\mathcal{I})$ is a YES instance of (P_D).

- If $\Phi(\mathcal{I})$ is a YES instance of (P_D), it exists then a solution $(x, \tilde{y}, w) \in \{0, 1\}^V \times \{0, 1\}^{E_\theta \times C} \times \{0, 1\}^{V \times C}$ of this instance of problem (P_D) with value less than or equal to Q. We define then vector $y \in \{0, 1\}^{E_\theta}$ as: $y_{ij} = \sum_{c \in C} y_{ij}^c$ for all $(i, j) \in E_\theta$. By construction, (x, y) is feasible for the instance \mathcal{I} of problem (R), and has value $\sum_{j \in J} c_j x_j + \rho \sum_{i \in I} (d_i + u_i)(1 - x_i)$ which is lower or equal to Q. It certifies that \mathcal{I} is a YES instance of (R_D).

Moreover the time complexity to compute $\Psi(\mathcal{I})$ is clearly polynomial in coding size of instance \mathcal{I} . □

One can legitimately question the interest of introducing relaxation (R) which is NP-hard, as the original problem (P) is. In fact, we will see in Sect. 6 that the commercial branch-and-bound algorithm that we used solves this relaxation considerably faster than (P), due to its smaller size and due to the absence of "big-M" constant in (R). This provides good and fast lower bounds on the value of problem (P).

5 | SOLUTION ALGORITHMS

To solve problem (P), we first used a standard MILP solver implementation (see Sect. 6). It turns out, however, that this commercial solver cannot solve all the tested instances to optimality with a practically reasonable time limit. This is why we also propose several heuristic algorithms, in order to find better solutions for the cases where the MILP solver does not close the optimality gap in due time.

5.1 | Greedy heuristics

The two first heuristic algorithms proposed here are based on a greedy approach. The second algorithm is a "multi-start" variant of the first one.

5.1.1 | First greedy heuristic

This algorithm sequentially treats the different available frequencies. For a given frequency, the following steps are repeated as long it is possible to generate a new cluster with a positive score:

- For each AP that is not turned-on yet, the clients that can be associated with it are selected in a greedy way. The construction of each potential cluster must respect the bandwidth limitation of the AP, and the interference caused by these new devices must not prevent pre-existing connections on the same frequency. A score is assigned to each potential cluster, made of gains of connecting the selected clients minus the AP cost.
- The cluster with highest score is selected, the corresponding devices are turned-on if and only if the score is nonnegative. If the score is negative, the channel is considered "full".

When the channel is "full", all devices switched on this channel are filtered out and the process is repeated for a new channel. In order to present a pseudo-code of this first greedy heuristic, we need to introduce three auxiliary procedures. In all these procedures, the variable ChannelEnv stands for "channel environment" and designates the set of APs already selected and switched on this channel, jointly with the client devices connected

Algorithm 1 Procedure **CompatibleDevice**

```

1: procedure CompatibleDevice(k, ChannelEnv)
2:   for each pair (i, j) of client-AP connection in ChannelEnv do
3:     Let  $N_{up}$  be the interference-plus-noise level for uplink connection (i, j) in ChannelEnv
4:     Let  $N_{down}$  be the interference-plus-noise level for downlink connection (i, j) in ChannelEnv
5:     if  $N_{up} + p_{kj} > K_{ij}^u$  then ▷ If the AP k hinders the (i,j) uplink connection.
6:       return FALSE
7:     end if
8:     if  $N_{down} + p_{ki} > K_{ij}^d$  then ▷ If the AP k hinders the (i,j) downlink connection.
9:       return FALSE
10:    end if
11:  end for
12:  return TRUE
13: end procedure

```

to them. Given a device index $k \in V$ and a “channel environment”, i.e. a set of pairs (client, AP), the first auxiliary procedure (Algorithm 1) aims at checking if turning-on device k is possible in the sense that it does not hinder a connection present in the environment. Given an AP that we denote by a , given a set of possible client devices and a “channel environment”, the second auxiliary procedure (Algorithm 2) aims at checking if AP a may be turned-on without impacting the existing connections already set on this channel, and then compute a set of client devices (a cluster) in a greedy approach, knowing that the connection possibilities also depend on the “channel environment”. This procedure returns the “score” of this cluster, i.e. its contribution to the [Objective Function \(12\)](#).

Thanks to the ScoreCluster procedure, the third auxiliary procedure (Algorithm 3) tests all the possible new clusters to add on a current channel

Algorithm 2 Procedure **ScoreCluster**

```

1: procedure ScoreCluster(a, I, ChannelEnv)
2:   if compatible-device(a, ChannelEnv) then
3:     Sort clients by decreasing order of  $d_i + u_i$ 
4:      $S \leftarrow C_a$ 
5:     ChannelEnv2  $\leftarrow$  ChannelEnv  $\cup$  {a}
6:      $\Gamma \leftarrow \gamma$ 
7:     for i in I do ▷ Loop adding client devices in the cluster.
8:       if  $d_i + u_i < \Gamma \wedge$  CompatibleDevice(i, env2) then
9:         Let  $N_{up}$  be the interference-plus-noise level for the (i, a) uplink connection in env2
10:        Let  $N_{down}$  be the interference-plus-noise level for the (i, a) downlink connection in env2
11:        if  $N_{up} \leq K_{ia}^u \wedge N_{down} \leq K_{ia}^d$  then ▷ If the connection (i, a) is possible.
12:           $S \leftarrow S - \rho(d_i + u_i)$ 
13:           $\Gamma \leftarrow \Gamma - (d_i + u_i)$ 
14:          ChannelEnv2  $\leftarrow$  ChannelEnv2  $\cup$  {i}
15:        end if
16:      end if
17:    end for
18:    return S, ChannelEnv2
19:  else
20:    return 0, ChannelEnv
21:  end if
22: end procedure

```

and select the “best” one, in a greedy approach too. With this auxiliary procedures we can now introduce Algorithm 4, [the pseudo-code of the](#)

Algorithm 3 Procedure **ClusterSelection**

```

1: procedure ClusterSelection( $I, J, \text{ChannelEnv}$ )
2:    $S \leftarrow 0$ 
3:    $\text{ChannelEnv2} \leftarrow \text{ChannelEnv}$ 
4:   for  $a$  in  $J$  do
5:      $S_{\text{aux}}, \text{ChannelEnvAux} \leftarrow \text{ScoreCluster}(a, I, \text{ChannelEnv})$ 
6:     if  $S_{\text{aux}} < S$  then
7:        $S \leftarrow S_{\text{aux}}$ 
8:        $\text{ChannelEnv2} \leftarrow \text{ChannelEnvAux}$ 
9:     end if
10:  end for
11:  return  $S, \text{ChannelEnv2}$ 
12: end procedure

```

Greedy Heuristic 1 (GH1). In this algorithm, the size of array patterns is $|\mathcal{C}|$, the number of available channels. At the end of the algorithm, $\text{patterns}[i]$ contains the list of (client, AP) pairs set on this channel.

Algorithm 4 Procedure **GreedyHeuristic1 (GH1)**

```

1: procedure GreedyHeuristic1( $I, J, \mathcal{C}$ )
2:    $\text{val} \leftarrow \rho \sum_{i \in I} (d_i + u_i)$ 
3:   Declare patterns as an array indexed by  $\mathcal{C}$ 
4:   for  $c$  in  $\mathcal{C}$  do ▷ Loop over the channels.
5:      $\text{ChannelEnv} \leftarrow \emptyset$ 
6:      $S, \text{ChannelEnv} \leftarrow \text{ClusterSelection}(I, J, \text{ChannelEnv})$ 
7:     while  $S < 0$  do
8:        $\text{val} \leftarrow \text{val} + S$ 
9:        $\text{patterns}[c] \leftarrow \text{ChannelEnv}$ 
10:       $I \leftarrow I \setminus \text{clients}(\text{ChannelEnv})$ 
11:       $J \leftarrow J \setminus \text{APs}(\text{ChannelEnv})$ 
12:       $S, \text{ChannelEnv} \leftarrow \text{ClusterSelection}(I, J, \text{ChannelEnv})$ 
13:    end while
14:  end for
15:  return  $\text{val}, \text{patterns}$ 
16: end procedure

```

5.1.2 | Multistart greedy heuristic

The idea of the **Greedy Heuristic 2 (GH2)** comes from the observation that the first selected AP in the previous greedy heuristic highly influences the final results. Hence, it is relevant to run several times the greedy heuristic with a different AP selected first in the process: at iteration $i \in \{0, J - 1\}$ of GH2, we run GH1 but with i AP positions being in the TabuList, i.e. that cannot be used for the first AP placed in GH1.

5.2 | Relaxation-based heuristics

We now present two heuristic algorithms based on the fact that the interference-free relaxation problem (R) presented in Sect. 3.2 is more efficiently solved by the used MILP solver than the original problem (P).

Algorithm 5 Procedure GreedyHeuristic2 (GH2)

```

1: procedure GreedyHeuristic2(I, J, C)
2:   TabuList  $\leftarrow$  []
3:   for  $i = 0, \dots, J - 1$  do
4:     Run GreedyHeuristic(I, J, C), but forbidding the APs in the TabuList for the first AP selection of the first channel.
5:      $A \leftarrow$  the first selected AP in the computed solution
6:     Append TabuList with A
7:   end for
8:   return Best encountered solution
9: end procedure

```

5.2.1 | First relaxation-based heuristic

The principle of this algorithm is to use the solution of the interference-free relaxation (R) to build a solution of the original problem (P), by assigning a channel to each cluster and possibly switching off the devices to make the solution feasible. Thus, this heuristic consists in successively solving two easier BLP problems:

1. **Positioning step:** Choose the AP-hosting candidate points, select the client devices to serve, and design "clusters" (set of client devices connected to a same AP) by solving the interference-free relaxation (R). This allows us to obtain a solution $(\bar{x}, \bar{y}) \in \{0, 1\}^V \times \{0, 1\}^{E_\theta}$ that represents clusters.
2. **Frequency assignment step:** Assigning channels to clusters and potentially turning-off devices if needed. We define this frequency assignment problem as the initial problem (P) with the (\bar{x}, \bar{y}) -based additional constraints:

$$\begin{aligned} x_i &\leq \bar{x}_i, \quad \forall i \in V \\ y_{ij} &\leq \bar{y}_{ij}, \quad \forall (i, j) \in E_\theta \end{aligned} \quad (24)$$

These constraints reduce the combinatorial nature of the problem by specifying that only devices and connections existing in (\bar{x}, \bar{y}) may be used in the final deployment. Introducing the set of allowable edges $E(\bar{y}) = \{(i, j) \in E_\theta : \bar{y}_{ij} = 1\}$, this frequency assignment problem $(P_{\bar{x}, \bar{y}})$ can be written in a compact way:

$$\begin{aligned} \min \quad & \sum_{j \in J} c_j x_j + \rho \sum_{i \in I} (d_i + u_i)(1 - x_i) \\ \text{s.t.} \quad & x_i \leq \bar{x}_i, \quad \forall i \in V \\ & \sum_{c \in C} w_{ic} = x_i, \quad \forall i \in V \\ & w_{ic} \leq w_{jc}, \quad \forall (i, j) \in E(\bar{y}), \forall c \in C \\ & \theta + \sum_{\substack{(k, l) \in E(\bar{y}) \\ l \neq j}} p_{ki} w_{kc} + \sum_{\substack{k \in J \\ k \neq j}} p_{ki} w_{kc} \leq K_{ij}^d + M(1 - w_{ic}), \quad \forall (i, j) \in E(\bar{y}), \forall c \in C \\ & \theta + \sum_{\substack{(k, l) \in E(\bar{y}) \\ l \neq j}} p_{kj} w_{kc} + \sum_{\substack{k \in J \\ k \neq j}} p_{kj} w_{kc} \leq K_{ij}^u + M(1 - w_{ic}), \quad \forall (i, j) \in E(\bar{y}), \forall c \in C \\ & \mathbf{x} \in \{0, 1\}^V, \mathbf{w} \in \{0, 1\}^{V \times C}. \end{aligned} \quad (P_{\bar{x}, \bar{y}})$$

This optimization problem has a number of variables and constraints linear in $|C| \times |V|$. Indeed we have $|E(\bar{y})| \leq V$. We underline that problem $(P_{\bar{x}, \bar{y}})$ does not only aim at assigning frequencies to each device of the relaxation solution (\bar{x}, \bar{y}) , but also at turning off devices to get a feasible solution of (P). From any (\mathbf{x}, \mathbf{w}) solution of $(P_{\bar{x}, \bar{y}})$, one can deduce a solution (\mathbf{x}, \mathbf{y}) of (P) by setting $y_{ij}^c = \bar{y}_{ij} w_{ic}$. This property is used in the following algorithms: for a matter of simplicity, we consider (\mathbf{x}, \mathbf{w}) and (\mathbf{x}, \mathbf{y}) as being equivalent, if the definition of \bar{y} is unambiguous.

With those definitions we can now introduce Algorithm 6, the pseudocode of the [Relaxation-based Heuristic \(RH1\)](#).

5.2.2 | Second relaxation-based heuristic

We introduce an iterative variant of the relaxation-based heuristic consisting in repeating positioning step and frequency assignment step alternately. The APs and clients positioning step is modified to benefit from the feedback of the frequency assignment step. We assume we have a threshold value $\tau \in \mathbb{R}_+$ and a non-negative vector $\phi \in \mathbb{R}_+^V$ and we are looking for a solution (\mathbf{x}, \mathbf{y}) of the relaxation problem (R) whose objective

Algorithm 6 Procedure **RelaxHeuristic1 (RH1)**

- 1: **procedure** RelaxHeuristic1(l, J, \mathcal{C})
- 2: Solve interference-free relaxation (R).
- 3: Let (\bar{x}, \bar{y}) be an optimal solution of the relaxation.
- 4: Solve the frequency assignment problem $P_{\bar{x}, \bar{y}}$.
- 5: Let sol be the optimal solution found and val be its value.
- 6: **return** val, sol
- 7: **end procedure**

value is lower than τ and with minimal score

$$\sum_{\substack{i \in V \\ x_i = 1}} \phi_i \quad \sum_{\substack{j \in V \\ \neg \exists H \in \mathcal{F}(\mathbf{y}) \text{ } i, j \in H}} p_{ji} \quad (25)$$

where $\mathcal{F}(\mathbf{y})$ denotes the set of clusters associated to deployment \mathbf{y} . We recall that a cluster is a set gathering an AP and all clients connected to it. Hence, the set $\mathcal{F}(\mathbf{y})$ is formally defined as

$$\mathcal{F}(\mathbf{y}) = \{ \{j\} \cup \{i \in I \mid y_{ij} = 1\} \mid j \in J, x_j = 1 \}. \quad (26)$$

The **Objective Function** (25) is chosen to come up with solution of the relaxation that avoid the overlapping of clusters. The problem of looking such a solution can be formulated as a BLP problem:

$$\begin{aligned}
& \min \sum_{i \in V} \phi_i n_i \\
& \text{s.t.} \quad \sum_{j \in J} c_j x_j + \rho \sum_{i \in I} (d_i + u_i)(1 - x_i) \leq \tau \\
& \quad \sum_{j \in J \mid (i,j) \in E_\theta} y_{ij} = x_i, \quad \forall i \in I \\
& \quad \sum_{i \in I \mid (i,j) \in E_\theta} (d_i + u_i) y_{ij} \leq \gamma x_j, \quad \forall j \in J \\
& \quad y_{ij} \leq x_j, \quad \forall (i,j) \in E_\theta \\
& \quad y_{ij} \leq x_i, \quad \forall (i,j) \in E_\theta \\
& \quad \sum_{j \in J, j \neq i} p_{ji} x_j + \sum_{j \in I} p_{ji} (x_j - y_{ji}) \leq n_i + M(1 - x_i), \quad \forall i \in J \\
& \quad \sum_{j \in J} p_{ji} (x_j - y_{ij}) + \sum_{(j,k) \in E_\theta} p_{ji} (y_{jk} - y_{ik}) \leq n_i + M(1 - x_i), \quad \forall i \in I \\
& \quad \mathbf{x} \in \{0, 1\}^V, \mathbf{y} \in \{0, 1\}^{E_\theta}, \mathbf{n} \in \mathbb{R}_+^V
\end{aligned} \quad (R_{\tau, \phi})$$

In this BLP model, the variable n_i represents the sum of the signal powers received by i and emitted by devices j that are not in the same cluster as i . Now that problem $(R_{\tau, \phi})$ is defined, we are able to present Algorithm 7, the **Relaxation-based Heuristic 2 (RH2)**. This algorithm depends on a parameter $r > 1$ that determines the increase of the penalty associated to a node that is turned off during the frequency assignment step. During this process, the parameter τ stores the current target for a solution value.

6 | COMPUTATIONAL EXPERIMENTS

This last section is dedicated to computational experiments that we led to assess the proposed methodology. We present the numerical setup for the simulation and the optimization parts, as well as the performance of both algorithmic steps.

6.1 | Instances generation

6.1.1 | Map generation and simulation

The first experimental step was to design building plans. Our solution to produce examples was to design **make-believe** building maps with a graphical raster editor. Table 7 introduces the physical coefficients for the simulation, that we used for all the maps. **First of all, we performed the simulations with two standard wavelengths for the IEEE 802.11 protocol: 2.4GHz and 5GHz.** Classically, the refractive index n_{air} of the ambient air was assimilated with the refractive index of the vacuum, i.e. 1. As concerns the refractive index n_{walls} of the walls, we took a classical value for the concrete [78] at a close frequency (50GHz), since the refractive index value for the specific frequencies 2.4GHz and 5GHz was not available. The diffusive coefficient α_{air} is null, since there is no absorption in the air; as regards the calibration of α_{walls} , we empirically chose the lowest value

Algorithm 7 Procedure RelaxHeuristic2 (RH2)

```

1: procedure RelaxHeuristic2( $l, J, \mathcal{C}, r$ )
2:   Solve interference-free (and channel free) relaxation (R).
3:   Let  $(\bar{x}, \bar{y})$  be the optimal solution found and  $\tau$  be its value.
4:   Solve the frequency assignment problem  $P_{\bar{x}, \bar{y}}$  associated with  $(\bar{x}, \bar{y})$  and let  $(\tilde{x}, \tilde{y})$  be its optimal solution found and  $v$  be its value.
5:    $\delta \leftarrow \min\{\min_j c_j, \min_i \rho(u_i + d_i)\}$ 
6:    $\text{Gap} \leftarrow v - \tau$ ,  $\text{nb\_it} \leftarrow \text{Gap}/\delta$ ,  $\phi \leftarrow 1$ 
7:   if  $\text{Gap} = 0$  then
8:     return  $v$ ,  $(\tilde{x}, \tilde{y})$ 
9:   end if
10:  for  $i = 1, \dots, \text{nb\_it}$  do
11:    Solve  $(R_{\tau, \phi})$  and let  $(\bar{x}, \bar{y})$  be the optimal solution found.
12:    Solve the frequency assignment problem  $P_{\bar{x}, \bar{y}}$  associated with  $(\bar{x}, \bar{y})$  and let  $(\tilde{x}, \tilde{y})$  be its optimal solution found and  $v$  be its value.
13:    if  $v \leq \tau$  then return  $v$ ,  $(\tilde{x}, \tilde{y})$ 
14:    else
15:       $\tau \leftarrow \tau + \delta$ 
16:      For any  $i \in V$  such that  $\bar{x}_i = 1$  and  $\tilde{x}_i = 0$ ,  $\phi_i \leftarrow r\phi_i$ 
17:    end if
18:  end for
19:  return Best encountered solution  $(\tilde{x}, \tilde{y})$  and its value.
20: end procedure

```

enabling to eliminate the fictitious interference patterns observed in simulation with a graphical display, when the walls behave like perfect mirror with no absorption (see Subject. 2.2). As concerns the AP emission power, we chose the value provided in the technical specifications of the Cisco Catalyst 9100 Wi-Fi 6 AP; the emission power for the client devices is taken one order of magnitude below.

Parameter	f_c	h	n_{air}	n_{walls}	α_{air}	α_{walls}	P_{AP}	P_{client}
Value	A: 2.4 GHz/ B: 5 GHz	3 cm	1	2.5	0 s/m ²	10 s/m ²	200 mW	10 mW

TABLE 7 Simulation parameters

We produced 6 different types of floors (MAP1, MAP2, MAP3, MAP4, MAP5, MAP6). The dimensions of such 2D maps are detailed in the Sect. 6.2. For each floor, we produced a one-level, a two-level and a three-level building based on this (duplicated) floor: hence, we obtained 18 different buildings. In order to calculate the field generated by devices on another floor, we used the field projection method (see Sect. 2.4) with an attenuation gain $g = 0.001 = -30\text{dB}$ per floor. Indeed we considered a 3cm-thick ceiling in concrete between floors: according to [78], the attenuation of the concrete is around -10dB/cm for frequencies in the GHz range.

For each building, the client and APs positions (2D coordinates and floor) were chosen at random. The choice of the discretization step h is consistent with the common knowledge in simulation, of using a step smaller than the wavelength (12.5cm for 2.4GHz and 6cm for 5GHz).

6.1.2 | Parameters of the optimization problems

We consider uniform uplink and downlink data flows demanded by the clients: the normalised data flows are $u_i = d_i = 0.5$. For each client, it corresponds to a full use of the bandwidth B in a balanced situation between uplink and downlink flow. The maximum flow capacity (normalized by the bandwidth) that an AP can process is set to $\gamma = 8$, meaning that an AP can handle at most 8 clients simultaneously. This number of clients per AP typically corresponds to a high-quality service requirement: the clients can have full use of their bandwidth at any time. We leave for future work the case where more customers per AP (up to 50) are tolerated, at the cost of a lower quality of service. According to Shannon's law (see Sect. 1.3) and using notations introduced in (2), the parameters K_{ij}^u and K_{ij}^d are taken in accordance to the normalised data rates and the signal strengths:

$$\begin{aligned}
 K_{ij}^u &= N_{\max}(u_i, 1, p_{ij}) = \frac{p_{ij}}{2^{u_i} - 1}, \\
 K_{ij}^d &= N_{\max}(d_i, 1, p_{ji}) = \frac{p_{ji}}{2^{d_i} - 1}.
 \end{aligned} \tag{27}$$

The value 0.1mW (resp. 0.01mW) for the noise parameter θ corresponds to the power of a client device attenuated by a 2cm-thick (resp. 3cm-thick) concrete wall, considering again, an attenuation of -10dB/cm [78]. This range for the noise thus corresponds to the presence of a client device emitting in an adjacent room.

We produced instances with uniform AP costs $c_j = c = 10$. We do not specify any monetary units for these costs since the dimension-free value c just serve as a reference with which we compare different values of ρ , the cost attributed with each client that is not covered. As concerns ρ , we considered two possible cases: either the deployer is indifferent between installing 1 AP and not covering 1 client ($\rho = c$) or the deployer wants to cover as many clients as possible, even if covering a client requires a fully dedicated AP ($\rho = 10c$). Table 8 presents 3 configurations for the pair of parameters (θ, ρ) . For the 18 building configurations, we tested each of the 3 sets of parameters presented in Table 8 with each of the two considered frequencies (2.4GHz and 5GHz), giving us a total of 108 cases. Finally, all of these 108 deployment cases were tested with a number of channels of 3 and 6, giving an total of 216 optimization problems. We now discuss the implementation and the results of the simulations in Sect. 6.2 and then the optimization algorithms in Sect. 6.3.

Set of parameters	θ	ρ
Set 0	0.01 mW	100
Set 1	0.01 mW	10
Set 2	0.1 mW	100

TABLE 8 Set of parameters

6.2 | Simulation experiments

6.2.1 | Implementation

The numerical experiments presented here were ran on a computer with the following characteristics:

- CentOS Linux 7 operating system;
- 32 processors Intel(R) Xeon(R) CPU E5-2620 v4 @ 2.10GHz;
- 64 GB of RAM.

We recall that the simulation process for a given building is in two steps: (i) we compute the LU factorization of the matrix A and (ii) based on this factorization, we solve $|I| + |J|$ linear systems $A\psi = F$ with the second member F corresponding to each possible emitting device position so as to compute the corresponding field. The LU factorization, as well as the linear system solution, are computed with linear algebra algorithms implemented in the *SuperLU* library [70], which is accessed through the Scipy wrapper [79] for Python. The simulation code, as well as the simulation instances and results are available online at the following link: github.com/aoustry/FDFDRadiowaveSimulator.

6.2.2 | Results

In Table 9, the column "LU decomposition time" corresponds to the computational time to perform a LU factorization of the matrix A in Eq. (8). The column "Solution time (average)" describes the average time required to compute, using the pre-computed LU decomposition, Ψ^i the solution of Eq. (8) for a RHS vector F^i corresponding to the emitting device $i \in V$. The column "Solution time (standard deviation)" corresponds to the standard deviation of the solution time of Eq. (8), for all the tested sources. The time for the field projection step on other floors (see Sect. 2.4), i.e. the time needed to compute $p_{ij} \leftarrow g^{|\text{floor}(i) - \text{floor}(j)|} |\Psi_j^i|$ for all $(i, j) \in V^2$, is less than 1s for all instances.

6.3 | Optimization experiments

6.3.1 | Implementation

All the optimization algorithms were implemented in the C++ programming language and ran on the same machine that the one used for the simulation experiments. We used a commercial MILP solver, namely IBM ILOG CPLEX 12.8 [80] that we called through the Concert Technology API for C++. At most 16 processors were allocated to CPLEX, and we set a time limit of 3600 seconds. For the implementation and solution

Floor type	Ground surface	N_x	N_y	LU decomposition time	Solution time (average)	Solution time (standard deviation)
Map 1	153 m ²	523	325	12 s	0.12 s	0.02 s
Map 2	293 m ²	1000	325	20 s	0.24 s	0.01 s
Map 3	472 m ²	898	584	49 s	0.53 s	0.03 s
Map 4	683 m ²	1200	632	74 s	0.65 s	0.02 s
Map 5	593 m ²	1067	618	63 s	0.66 s	0.03 s
Map 6	817 m ²	1230	738	120 s	0.72 s	0.03 s

TABLE 9 Simulation results

of the MILP problem (P), we noticed that using the CPLEX logical constraint feature, that compute dynamically the best “Big-M” to use, led to better results than the model with a pre-determined “Big-M” equals to $\theta + \sum_{(i,j) \in V^2} p_{ij}$. Similarly for the implementation of $(P_{\bar{x}, \bar{y}})$ and $(R_{\tau, \phi})$, we used the CPLEX logical constraint feature to compute automatically the “Big-M” constants. As concerns the heuristics, we also set a time limit of 3600 seconds, but this limit is never reached in the experiments. For the iterative relaxation-based heuristic RH2, we calibrated the choice of the parameter r by doing preliminary experiments, testing $r \in \{1.2, 1.5, 2, 3, 4\}$. As illustrated in Appendix, it appeared that the performance of this algorithm was not very sensitive to the choice of r . We chose the value $r = 3$, that seemed to be slightly better, although we cannot say that this advantage is statistically significant. The implementation of all the presented algorithms, as well as the optimization instances and full tables of results, including the preliminary tests for the choice of r , are available online at the following link: github.com/aoustry/Odewine.

6.3.2 | CPLEX performance

We start by presenting the numerical results obtained with the B&B algorithm of the solver CPLEX v12.8. We notice that CPLEX is able to find a global minimum within the time limit (3600s) for 96 instances out of 108 with the 3-channel configuration, i.e. 89% of the cases, and 100 instances out of 108 with the 6-channel configuration, i.e. 94% of the cases. In total, the average solution time for CPLEX is 480s, with a standard deviation of 1100s; the median solution time is only 4.3s. So as to visualize the solution time distribution more in detail, Figure 4 presents the performance profile, i.e. the number of instances (in y-axis) that requires less than t seconds (in x-axis) to be solved to global optimality by CPLEX. For instance, we see that around 80 instances with 6 channels (dark curve) require less than 20s to be solved to global optimality. Figure 2 shows a linear relation between the logarithm of the solution time and the instance size, i.e. the total number of clients and candidates; in other words, this reflects an exponential relation between the solution time and the instance size.

In the scatter plot displayed in Figure 3, each point represents, for a given instance (building and parameters $f_c/\rho/\theta$) the solution time for the 3-channel configuration (in x-axis) and for the 6-channel configuration (in y axis). We see that for many instances, these computational times are very similar, since the cluster of points fits very well the $y = x$ line on the left-hand side of the chart. Yet, for the most difficult instances (on the right-hand side of the chart), we see that the cluster is clearly below the $y = x$ line, meaning that the 6-channel configuration seems easier to solve; this corroborates the observation that the rate of globally solved instances is higher for the 6-channel configuration. Focusing on the unsolved cases, Figure 4 represents the cumulative distribution of the optimality gap, for the 3-channel and 6-channel configuration. It displays the number of instances (in y-axis) for which the optimality gap obtained by CPLEX is less than a given value (in x-axis). For instance, we see that the duality gap is less than 20% for 106 instances in the 3-channels configuration and also for 106 instances in the 6-channels configuration. We also see that for the 4 remaining cases, the optimality gap is very important (more than 80%).

We now turn to the performance analysis of the heuristic algorithms. We start by comparing the Greedy Heuristic GH1 with its iterative variant GH2, then the Relaxation-based Heuristic RH1 with its iterative variant RH2, to evaluate if it is worthwhile to increase the sophistication of these heuristics. Finally, we compare the heuristics with CPLEX.

6.3.3 | Comparison of the greedy heuristics

In this paragraph, we compare the two greedy heuristics: the basic version (Algorithm GH1) and the iterative version (Algorithm GH2). We will show that Algorithm GH2 presents a real advantage compared to Algorithm GH1.

First we emphasize that, by design of Algorithm GH2, the best objective value computed by Algorithm GH2 is necessarily lower than Algorithm GH1: if we move from GH1’s solution to GH2’s solution, the objective value is thus necessarily improving. We are now going to demonstrate that this improvement is statistically significant over the test set. In the following, what we call the “relative improvement of the objective value” is the

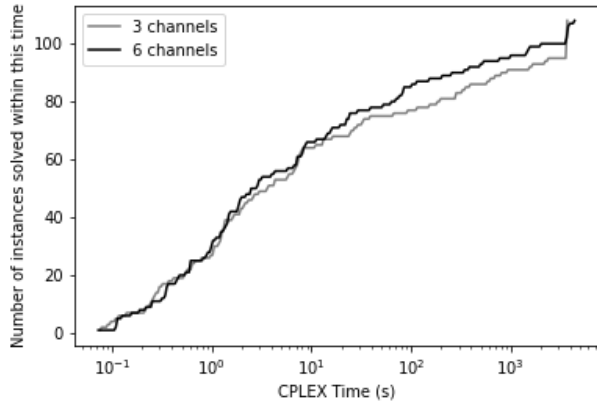


FIGURE 1 CPLEX v.12.8 performance profile

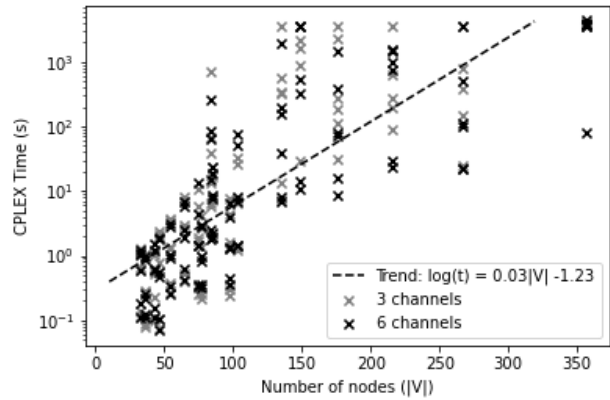


FIGURE 2 CPLEX v.12.8 solution time versus instance size

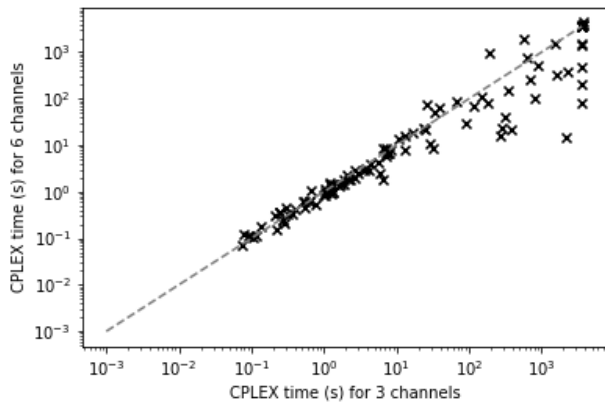


FIGURE 3 Time for 3 channels vs. Time for 6 channels

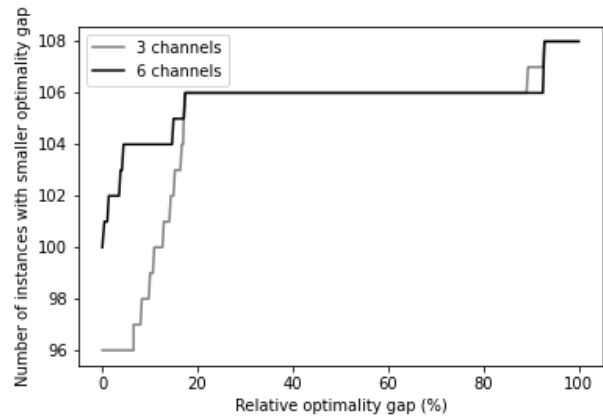


FIGURE 4 CPLEX v.12.8 optimality gap distribution

ratio $\frac{obj(GH1) - obj(GH2)}{obj(GH1)}$ expressed in %, where obj designates the best objective value. Table 10 shows that in average, the relative improvement of the objective value from GH1 to GH2 is 11%; the median relative improvement is 6%. For a tenth of the instances, the relative improvement of the objective value is more than 30%. To estimate the statistical significance of these observations, we performed a Wilcoxon signed-rank test on the best objective value series of GH1 and GH2 (over all instances); we obtained a p-value of the order of 10^{-25} , meaning that the null hypothesis "The two distributions are equal" can be rejected with very high confidence. To better visualize the distribution of the relative objective improvement

Statistic	Avg.	Std. dev.	Min.	Q 25%	Q 50%	Q 75%	Q 90%	Max
Value	11%	15%	0%	0%	6%	16%	30%	87%

TABLE 10 Statistics of the relative objective improvement from GH1 to GH2.

offered by the iterative version of the algorithm, Figure 5 presents a histogram for the 3-channel configuration and for the 6-channel configuration. We see that the shape of the distribution is quite similar for both numbers of channels, meaning that algorithm GH2 has a significant impact on the objective function in both configurations. Yet, we see more extreme values (above 70% of improvement) for the 3-channel configuration, meaning that the question of the robustness of these heuristics seems even more important in this configuration of scarce channel resource, where the frequency assignment plays an important role. Figure 6 is a scatter plot of the relative objective improvement as a function of the size of the instances. We see that the relative spread between the best objective value computed by GH1 and the best objective value computed by GH2 is

substantial for all instance sizes. The Pearson correlation index between the relative improvement and the instance sizes is 0.19, which denotes a weak but positive correlation. This lets us think that the advantage of GH2 w.r.t. GH1 in terms of objective value may still be significant for larger instances.

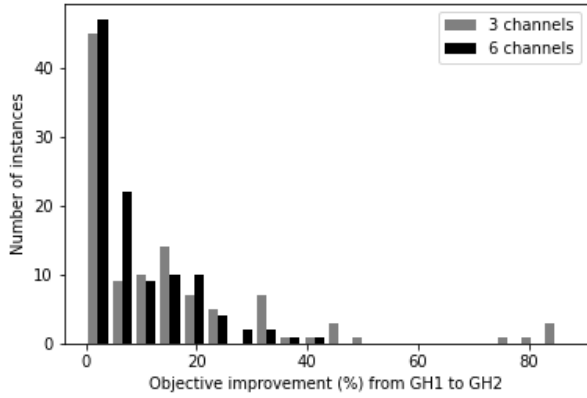


FIGURE 5 Histogram of objective improvement

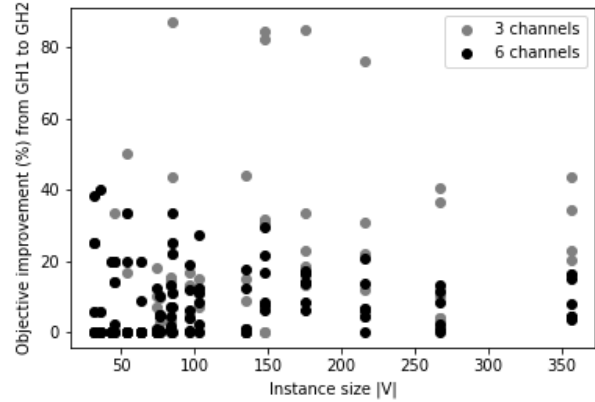


FIGURE 6 Objective improvement and instance size

Another point of comparison of the two greedy algorithms is their execution time: Algorithm GH2 is certainly more efficient in terms of objective value, but at what computational cost? The performance curve in Figure 7 shows the number of instances that require less than a given amount of time (in x-axis) to be solved by GH1, and by GH2. We clearly see that GH2's performance curve is positioned to the right of the GH1's curve, meaning that GH2's execution time is greater. For instance, around 200 instances require less than 0.1s of execution time for GH1, whereas 200 instances require less than 10s of execution time for GH2; the maximal execution time is 0.2s for GH1 and 34s for GH2. Nevertheless, the additional computational time of GH2 w.r.t. GH1 is less than 2s for the large majority of the instances, as illustrated by Figure 8 ; the maximum time difference between the two algorithms is 34s. Hence, we can consider that this increase in computation time remains limited and is worthwhile, in light of the improvements achieved by the GH2 algorithm for the objective function.

6.3.4 | Comparison of the relaxation-based heuristics

In this paragraph, we compare the two relaxation-based heuristics: the basic version RH1 and the iterative version RH2. We will show that for a limited number of cases, Algorithm RH2 allows a great improvement of the objective function w.r.t. the solution of Algorithm RH1.

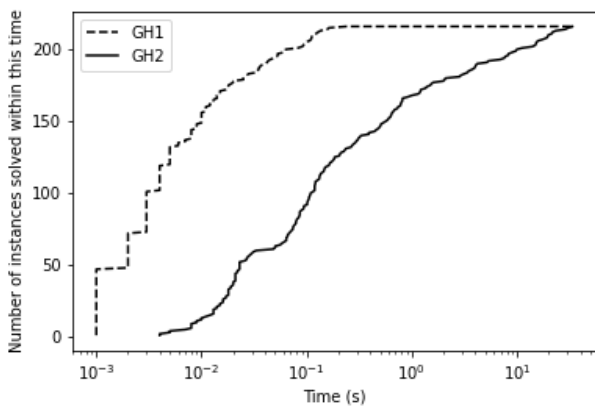


FIGURE 7 Performance curve of GH1 and GH2

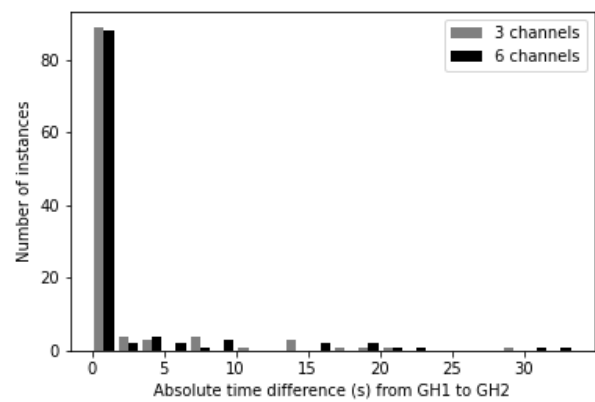


FIGURE 8 Histogram of time difference between GH1 and GH2

In a similar way to the greedy heuristics, we emphasize first that, by design of Algorithm RH2, the best objective value computed by Algorithm RH2 is necessarily lower than Algorithm RH1: if we move from RH1's solution to RH2's solution, the objective value is thus necessarily improving. In the following, what we call the "relative improvement of the objective value" is the ratio $\frac{\text{obj}(\text{RH1}) - \text{obj}(\text{RH2})}{\text{obj}(\text{RH1})}$ expressed in %. Table 11 shows that, in average, the objective value's relative improvement from Algorithm RH1 to Algorithm RH2 is 7%. As illustrated by Figure 9, the distribution of the objective value's relative improvement is skewed to the left, meaning that the improvement is null for many instances, but there are several instances for which it is large. More precisely, both Algorithm RH1 and Algorithm RH2 yield the same value for more than 3 instances out of 4; yet, for 1 instance over 10, the relative improvement is more than 30%. These major improvements yielded by Algorithm RH2 mainly occur for cases with 3 available channels (see Figure 9), but regardless of the instance size (see Figure 10).

So as to assess the statistical significance of these observations, we also performed a Wilcoxon signed-rank test on the best objective value series of Algorithm RH1 and Algorithm RH2 (over all instances); we obtained a p-value of the order of 10^{-9} , meaning that the null hypothesis "The two distributions are equal" can be rejected with very high confidence.

Statistic	Avg.	Std. dev.	Min.	Q 25%	Q 50%	Q 75%	Q 90%	Max.
Value	7%	18%	0%	0%	0%	0%	30%	93%

TABLE 11 Statistics of the relative objective improvement from RH1 to RH2.

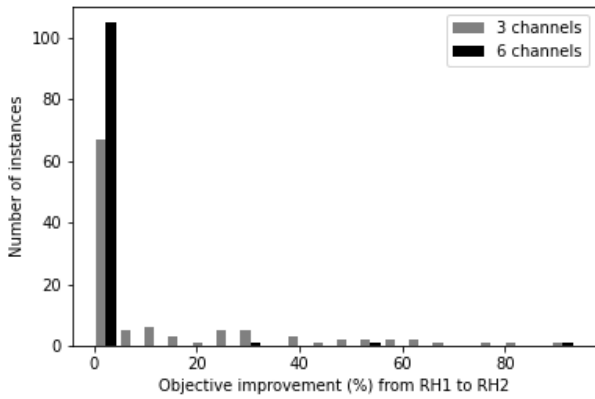


FIGURE 9 Histogram of objective improvement

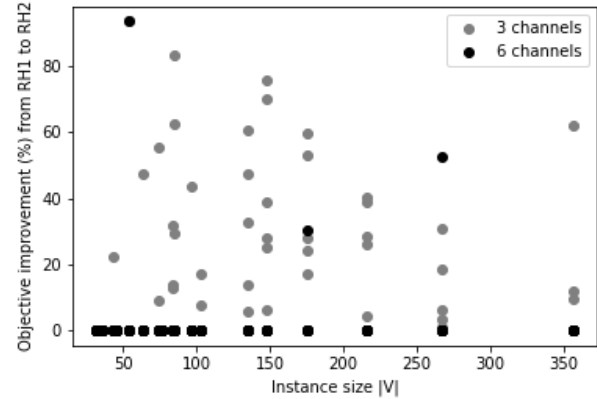


FIGURE 10 Objective improvement and instance size

As regards the computational time, the performance profiles (see Figure 11) of Algorithm RH1 and Algorithm RH2 are fitting well on the left hand side of the curve: for 1 instance over 2, the computational time of both algorithms is less than 0.2s. On the right hand side of the curve (highest computational times), the difference between the two algorithms is more important. For instance, 200 instances are solved by RH1 in less than 10 seconds, whereas the equivalent time threshold is 100 seconds for RH2. In average, the additional computation time of Algorithm RH2 w.r.t. Algorithm RH1 is 27s, with a standard deviation of 184s. In only 2 cases, this computational time difference exceeds 800s. Over all instances, the maximum computation time for RH2 is around 2500s, which is below the maximum time limit that we set. Thus, we can conclude that given the time limit we have set, Algorithm RH2 is worth using, despite its longer time w.r.t. Algorithm RH1, because it potentially allows, for some cases, to drastically improve the result of the RH1 algorithm.

6.3.5 | CPLEX vs. iterative heuristics

We conclude the presentation of our numerical experiments with a comparison of the results given by CPLEX and those given by the heuristics. For the sake of readability, we only include the heuristic Algorithms GH2 and RH2 in this comparative analysis; this makes sense since we demonstrated in the previous paragraphs the superiority of the iterative versions of the heuristics (Algorithm GH2 and RH2) over their baseline versions (Algorithm GH1 and RH1) in terms of objective value.

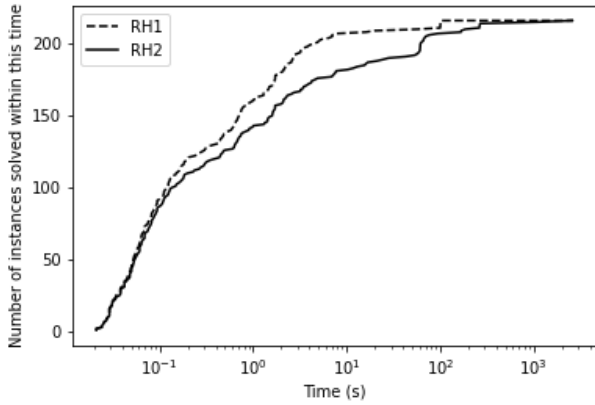


FIGURE 11 Performance curve of RH1 and RH2

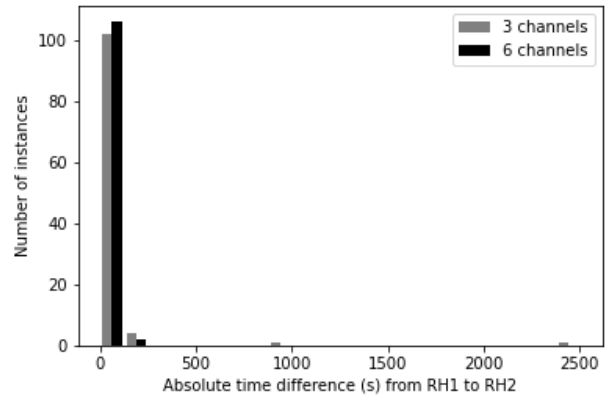


FIGURE 12 Histogram of time difference between RH1 and RH2

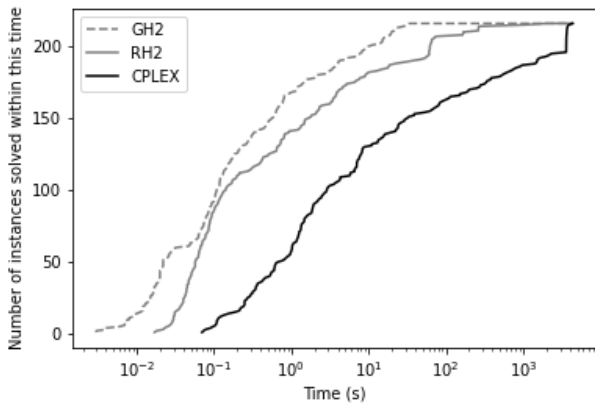


FIGURE 13 Performance curve of GH2, RH2 and CPLEX

Time statistic	Avg.	Std. dev.	Q 25%	Q 50 %	Q 75 %
GH2	2.6s	5.6s	0.02s	0.12s	0.78s
RH2	28s	160s	0.06	0.19s	3.4s
CPLEX	480s	120s	0.94s	4.29s	93s

FIGURE 14 Time statistics

We first compare the computation time. The performance profiles in Figure 13 clearly show that the time distribution of Algorithm GH2 lies to the left of Algorithm RH2's time distribution, which lies to the left of CPLEX's time distribution. For instance, 168 instances are solved by Algorithm GH2 in less than 1s, 141 instances are solved by Algorithm RH2 in less than 1s and only 57 instances are solved by CPLEX in less than 1s. The average, the standard deviation and some quantiles of the computing time are available in Figure 14. To assess the statistical significance of these findings, we perform two Wilcoxon signed-rank tests. The first one compares the time distributions of GH2 and RH2; the second one compares the time distributions of RH2 and CPLEX. In both cases, the obtain lower bound is below 10^{-7} , meaning that the null hypothesis ("The two distributions are equal") can be ruled out.

Figure 15 (resp. Figure 16) shows the histogram of the relative objective value advantage of CPLEX over the heuristics in the 3-channel (resp. 6-channel) configuration; more precisely, the relative advantage of CPLEX over GH2 is computed as $\frac{\text{val}(\text{GH2}) - \text{val}(\text{CPLEX})}{\text{val}(\text{CPLEX})}$ and expressed in %, and similarly for RH2. A positive value means that CPLEX is better, a negative value means that the heuristic is better. In the 3-channel configuration, we see that the heuristic algorithms provides as good solutions as CPLEX in more than 70 cases. Yet, they also appear to provide bad solutions with more than 100% gap w.r.t. CPLEX solution. In this respect, the Algorithm GH2 seems more robust than Algorithm RH2, since it returns less solutions with a optimality gap w.r.t CPLEX solution that is higher than 50%: there are 4 such cases for GH2 but 14 for RH2. Looking at Figure 16, we see that the heuristics are more robust in the 6-channel configuration: the maximal optimality gap of the heuristic is much lower (less than 30%). In this configuration, Algorithm RH2 appears to be better than GH2, since it finds a solution that is as good as CPLEX's solution (or strictly better) in 107 cases over 108: this seems natural, since the interference-free relaxation is more likely to yield feasible deployment in the 6-channel configuration than in the 3-channel configuration. As concerns Algorithm GH2, it finds a 6-channel solution that is as good as CPLEX's solution

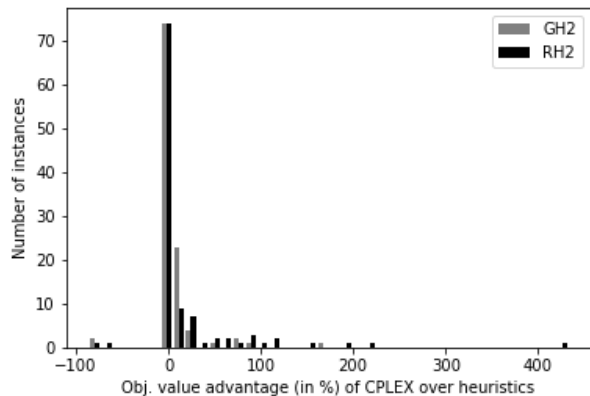


FIGURE 15 Obj. value advantage of CPLEX over the Algorithms GH2 and RH2 (3 channels)

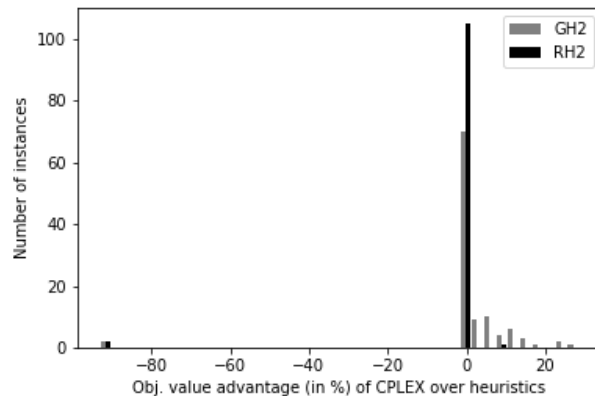


FIGURE 16 Obj. value advantage of CPLEX over the Algorithms GH2 and RH2 (6 channels)

(or strictly better) in 66 instances. These observations in both 3-channel and 6-channel configurations suggest that neither of the two iterative heuristics dominates the other; rather they are complementary.

Finally, Table 12 presents the numerical results obtained for the open cases, for which the best upper bound is strictly greater than the best lower bound obtained. We remark first that despite the 3600s time limit, CPLEX may take a longer computational time: the solution process seems not to be immediately stopped by CPLEX when the time limit is reached. In 4 cases (Instance_MAP6A_2_3 and Instance_MAP6B_2_3 with 3 or 6 channels), we observe that the objective values computed by the heuristic algorithms are clearly better than CPLEX's solution value, with a relative improvement greater than 80%. A posteriori, we remark that the case Instance_MAP6B_2_3 with 6 channels is solved: since the lower bound computed by CPLEX is 1231.3 and since the only possible objective values in our instances are multiples of 10 since $c = 10$ and $\rho(u_i + d_i) = c$ or $10c$, this means that 1240 is a valid lower-bound; Precisely, Algorithm RH2 finds a solution with value 1240, which is thus optimal. These observations suggest that in cases where CPLEX is not able to close the optimality gap, the proposed heuristics have a real interest because they allow to find potentially better solutions. This is not systematically the case, but considering the low execution time of the heuristics compared to CPLEX, it is worth running these heuristics to try beating CPLEX's incumbent solution. This seems all the more relevant as the size of the deployment increases. Table 12 also shows that neither of the iterative heuristics seems to dominate the other, and again, seem complementary.

7 | CONCLUSION

We proposed a protocol to optimize the deployment of a WLAN, taking full account of the building's architecture, which we tested on mid-size buildings with a floor area of up to 1000m² and several floors. The strength of our approach is a sophisticated but fast to code simulator that is based on the physical equations of radio wave propagation. This simulator allows us to calculate the electromagnetic field produced by any source in the building. We then introduce a stylized network deployment optimization problem, which consists of optimizing the positioning and frequency assignment of the APs to provide WiFi access to customers whose positions are given. This problem, which is formulated as a BLP, has the particularity of fully exploiting the data produced by the radio propagation simulator. We show that this problem is strongly NP-difficult, and the extensive numerical experiments that we have carried out with a standard MILP solver implementation have confirmed the difficulty of the problem, in the sense that the execution time seems to increase exponentially with the instance size. This commercial solver was typically able to solve, within one hour, 196 instances over 216. Within this time limit, the optimality gap could exceed 80% for the largest instances encountered, with more than 300 nodes. This is the reason why we also proposed several heuristic algorithms: a greedy heuristic and its iterative variant; and another heuristic based on a natural relaxation of the original problem, and its iterative variant. We identified that the iterative heuristics clearly outperforms their baseline counterpart. We also observed that neither the iterative greedy algorithm or the iterative relaxation-based algorithm dominates the other in terms of objective value: the first one seems more robust in a context with a limited number of channels, the second one is more robust in a context with abundant channel resources. The two of these heuristic algorithms find better solutions than the commercial solver for some of the largest instances. This illustrates the interest of the developed heuristic algorithms, whose computation time is, moreover, clearly lower than the exact approach.

Instance name	V	C	Time (s)			Lower bound		Best solution value		
			CPLEX	GH2	RH2	CPLEX	CPLEX	GH2	RH2	
Instance_MAP5A_1_1	148	3	3603	<1	61	123.8	150	150	150	
Instance_MAP5A_2_3	216	3	3614	3	65	177.5	190	190	380	
Instance_MAP6A_0_3	176	3	3610	1	72	228.8	250	280	1330	
Instance_MAP6A_1_3	267	3	3624	7	74	708.8	830	870	1600	
Instance_MAP6A_2_1	356	3	3677	18	2009	347.9	400	460	470	
Instance_MAP6A_2_2	356	3	3612	21	263	2854.9	3430	4430	5100	
Instance_MAP6A_2_3	356	3	3683	15	1032	1231.3	11910	2970	2140	
Instance_MAP5B_1_1	148	3	3602	<1	60	123.8	150	150	150	
Instance_MAP6B_1_3	267	3	3620	7	167	710.0	840	870	1780	
Instance_MAP6B_2_1	356	3	3635	19	167	373.4	420	460	490	
Instance_MAP6B_2_2	356	3	3610	29	263	2880.000	3210	4120	5100	
Instance_MAP6B_2_3	356	3	3682	15	268	1231.3	17920	2570	5910	
Instance_MAP5A_1_1	148	6	3608	<1	<1	123.8	150	150	150	
Instance_MAP6A_1_3	267	6	3664	9	3	708.8	720	760	720	
Instance_MAP6A_2_1	356	6	3753	22	5	345.4	360	400	360	
Instance_MAP6A_2_2	356	6	3642	31	265	2320.0	2330	2390	2510	
Instance_MAP6A_2_3	356	6	4362	20	9	1231.3	17920	1280	1240	
Instance_MAP5B_1_1	148	6	3608	<1	<1	127.5	150	150	150	
Instance_MAP6B_2_1	356	6	3729	23	4	371.8	390	440	390	
Instance_MAP6B_2_3	356	6	3893	20	18	1231.3	17920	1280	1240	

TABLE 12 Numerical results for the open instances

In future work we will be able to test our simulator for even larger buildings, albeit at the cost of longer computation times. Future work will also consist of testing the different optimization algorithms, exact or heuristic, for even larger instances so as to get closer to the thousand, regarding the cumulated number of clients and APs. It is likely that such cases would confirm the relevance of using heuristic algorithms. Another future research line is to implement an exact approach that can better scale, as a column-generation algorithm for instance. Finally, we also plan to propose a stochastic or robust variant of this optimization problem to take into account several scenarios concerning the use of the network or the presence of moving obstacles in the building.

ACKNOWLEDGEMENTS

This work was mainly funded by the Cisco Foundation Grant URP n. 594955. Two of the authors (CD, LL) are also partly supported by the European Union's Horizon 2020 research and innovation programme under the Marie Skłodowska-Curie grant agreement n. 764759 "MINOA".

References

- [1] P. Calégari, F. Guidec, P. Kuonen and B. Chamaret and S. Ubéda and S. Josselin and D. Wagner and M. Pizarosso, *Radio network planning with combinatorial optimization algorithms*. ACTS Mobile Telecommunications Summit, 1996, 707-713.
- [2] I. Akyildiz, W. Su and Y. Sankarasubramaniam and E. Cayirci, *Wireless sensor networks: a survey*, Computer networks **38** (2002), 393-422.
- [3] B. Das and V. Bharghavan, *Routing in ad-hoc networks using minimum connected dominating sets*, International Conference on Communications, IEEE, 1999, 376-380.
- [4] G.-H.Lin and G. Xue, *Steiner tree problem with minimum number of Steiner points and bounded edge-length*, Information Processing Letters **69** (1999),53-57.

- [5] D. Chen, D.-Z. Du, X.-D. Hu, G.-H. Lin, L. Wang and G. Xue, *Approximations for Steiner trees with minimum number of Steiner points*, Journal of Global Optimization **18** (2000), 17–33.
- [6] M. Min, H. Du, X. Jia, C. Huang, S. Huang and W. Wu, *Improving construction for connected dominating set with Steiner tree in wireless sensor networks*, Journal of Global Optimization **35** (2006), 111–119.
- [7] M. Rebai, H. Snoussi, F. Hnaïen and L. Khoukhi, *Sensor deployment optimization methods to achieve both coverage and connectivity in wireless sensor networks*, Computers & Operations Research **59** (2015), 11–21.
- [8] S. Elloumi, O. Hudry, E. Marie, A. Plateau and S. Rovedakis, *Optimization of wireless sensor networks deployment with coverage and connectivity constraints*. 4th International Conference on Control, Decision and Information Technologies, IEEE, 2017, 336–341.
- [9] C. Bentz, M.-C. Costa and A. Hertz. On the edge capacitated Steiner tree problem, Working paper, 2019. <https://hal.archives-ouvertes.fr/hal-01465403/document>.
- [10] G. Di Caro and E. Flushing, *Optimal relay node placement for throughput enhancement in wireless sensor networks*, 50th FITCE Congress ICT: Bridging an Ever Shifting Digital Divide, IEEE, 2011, 1–6.
- [11] Y. Hou, Y. Shi, H. Sherali and S. Midkiff, *Prolonging sensor network lifetime with energy provisioning and relay node placement*, Second Annual Communications Society Conference on Sensor and Ad Hoc Communications and Networks, IEEE, 2005, 295–304.
- [12] G. Wang, L. Huang, H. Xu and J. Li, *Relay node placement for maximizing network lifetime in wireless sensor networks*, 4th International Conference on Wireless Communications, Networking and Mobile Computing, IEEE, 2008, 1–5.
- [13] T. Rault, A. Bouabdallah and Y. Challal, *Energy efficiency in wireless sensor networks: A top-down survey*, Computer Networks **67** (2014), 104–122.
- [14] K. Aardal, S. van Hoesel, A. Koster, C. Mannino and A. Sassano, *Models and solution techniques for frequency assignment problems*, Annals of Operations Research **153** (2007), 79–129.
- [15] E. Amaldi, A. Capone, F. Malucelli and C. Mannino, “*Optimization problems and models for planning cellular networks*”, *Handbook of Optimization in Telecommunications*, Springer, Boston, 2006, 917–939.
- [16] C. Lee and H. Kang, *Cell planning with capacity expansion in mobile communications: A tabu search approach*, Transactions on Vehicular Technology **49** (2000), 1678–1691, .
- [17] R. Akl, M. Hegde, M. Naraghi-Pour and P. Min, *Multicell CDMA network design*, Transactions on Vehicular Technology **50** (2001), 711–722.
- [18] R. Mathar and M. Schmeink, *Optimal base station positioning and channel assignment for 3G mobile networks by integer programming*, Annals of Operations Research **107** (2001), 225–236.
- [19] D. Catrein, L. Imhof and R. Mathar, *Power control, capacity, and duality of uplink and downlink in cellular CDMA systems*, Transactions on Communications **52**,(2004), 1777–1785.
- [20] E. Amaldi, A. Capone, F. Malucelli and F. Signori, *UMTS radio planning: Optimizing base station configuration*, Proceedings of 56th Vehicular Technology Conference, volume 2, IEEE, 2002, 768–772.
- [21] E. Amaldi, A. Capone and F. Malucelli, *Planning UMTS base station location: Optimization models with power control and algorithms*, Transactions on Wireless Communications **5** (2003), 939–952.
- [22] E. Amaldi, P. Belotti, A. Capone and F. Malucelli, *Optimizing base station location and configuration in UMTS networks*, Annals of Operations Research, **146** (2006), 135–151.
- [23] M. Alsharif and R. Nordin, *Evolution towards fifth generation (5G) wireless networks: Current trends and challenges in the deployment of millimetre wave, massive MIMO, and small cells*, Telecommunication Systems, **64** (2017), 617–637.
- [24] P. Seda, M. Seda, and J. Hosek, *On Mathematical Modelling of Automated Coverage Optimization in Wireless 5G and beyond Deployments*, Applied Sciences, **10**(2020), 8853.

- [25] F. Musumeci, C. Bellanzon, N. Carapellese, M. Tornatore, A. Pattavina and S. Gosselin, *Optimal BBU Placement for 5G C-RAN Deployment Over WDM Aggregation Networks*, in *Journal of Lightwave Technology*, **34** (2016), 1963–1970.
- [26] G. V. Arévalo, M. Tipán and R. Gaudino, *Techno-Economics for Optimal Deployment of Optical Fronthauling for 5G in Large Urban Areas*, 20th International Conference on Transparent Optical Networks, 2018, 1–4.
- [27] H. Chen, Y. Mo, Q. Qian and P. Xia, *Research on 5G Wireless Network Deployment in Tourist Cities*, International Wireless Communications and Mobile Computing, 2020, 398-402.
- [28] H. Ganame, L. Yingzhuang, H. Ghazzai, and D. Kamissoko, *5G base station deployment perspectives in millimeter wave frequencies using meta-heuristic algorithms*. *Electronics*, **8**(2019), 1318.
- [29] F. Han, S. Zhao, L. Zhang, and J. Wu, *Survey of strategies for switching off base stations in heterogeneous networks for greener 5G systems*, *IEEE Access*, **4** (2016), 4959–4973.
- [30] Y. Lee, K. Kim and Y. Choi, *Optimization of AP placement and channel assignment in wireless LANs*, 27th Annual Conference on Local Computer Networks, IEEE, 2002, 831–836.
- [31] A. Gondran, O. Baala, A. Caminada and H. Mabed, *Joint optimization of access point placement and frequency assignment in WLAN*, 3rd International Conference in Central Asia on Internet, IEEE, 200, 1–5.
- [32] A. Eisenblatter, H.-F. Geerdes and I. Siomina, *Integrated access point placement and channel assignment for wireless LANs in an indoor office environment*. *IEEE International Symposium on a World of Wireless, Mobile and Multimedia Networks*, IEEE, 2007, 1–10.
- [33] A. Farsi, N. Achir and K. Boussetta, *WLAN planning: Separate and joint optimization of both access point placement and channel assignment*, *Annals of Telecommunications* **70** (2015), 263–274.
- [34] E. Ben Hamida, G. Chelius and J.-M. Gorce, *Impact of the physical layer modeling on the accuracy and scalability of wireless network simulation*, *Simulation*, **85** (2009), 574–588.
- [35] S. Seidel and T. Rappaport, *914 MHz path loss prediction models for indoor wireless communications in multifloored buildings*, *Transactions on Antennas and Propagation* **40** (1992), 207–217.
- [36] S. Seidel and T. Rappaport, *Site-specific propagation prediction for wireless in-building personal communication system design*, *Transactions on Vehicular Technology*, **43** (1994), 879–891.
- [37] K.-W. Cheung, J.-M. Sau and R. Murch, *A new empirical model for indoor propagation prediction*, *Transactions on Vehicular Technology* **47** (1998), 996–1001.
- [38] T. Rappaport et al, *Wireless Communications: Principles and Practice*, IEEE Press, Upper Saddle River, 1996.
- [39] R. Valenzuela, S. Fortune and J. Ling, *Indoor propagation prediction accuracy and speed versus number of reflections in image-based 3D ray-tracing*, 48th Vehicular Technology Conference, **1**, IEEE, 1998, 539–543.
- [40] S. Fortune, *Efficient algorithms for prediction of indoor radio propagation*, 48th IEEE Vehicular Technology Conference, vol. 1. IEEE, 1998, 572–576.
- [41] C.-F. Yang, B.-C. Wu and C.-J. Ko, *A ray-tracing method for modeling indoor wave propagation and penetration*, *Transactions on Antennas and Propagation* **46** (1998), 907–919.
- [42] M. Hassan-Ali and K. Pahlavan, *A new statistical model for site-specific indoor radio propagation prediction based on geometric optics and geometric probability*, *Transactions on Wireless Communications* **1** (2002), 112–124.
- [43] G. Athanasiadou and A. Nix, *Investigation into the sensitivity of the power predictions of a microcellular ray tracing propagation model*, *Transactions on Vehicular Technology* **49** (2000), 1140–1151.
- [44] F. Agelet, A. Formella, J.-M. Rabanos, F. De Vicente and F. Fontan, *Efficient ray-tracing acceleration techniques for radio propagation modeling*, *Transactions on Vehicular Technology* **49** (2000), 2089–2104.

- [45] Z. Yun, Z. Zhang and M. Iskander, *A ray-tracing method based on the triangular grid approach and application to propagation prediction in urban environments*, Transactions on Antennas and Propagation **50** (2002), 750–758.
- [46] L. Talbi and G. Delisle, *FDTD characterization of the Indoor Propagation*, Journal of Electromagnetic Waves and Applications **10** (1996), 243–247.
- [47] J. Lee and A. Lai, *FDTD analysis of Indoor Radio Propagation*, Antennas and Propagation Society International Symposium, vol. 3, IEEE, 1998, 1664–1667.
- [48] B. Chopard, P. Luthi and J.-F. Wagen, *Lattice Boltzmann method for wave propagation in urban microcells*, Proceedings - Microwaves, Antennas and Propagation, vol. 144, IEEE, 1997, 251–255.
- [49] J.-M. Gorce, K. Jaffres-Runser and G. De La Roche, *Deterministic approach for fast simulations of indoor radio wave propagation*, Transactions on Antennas and Propagation **55** (2007), 938–948.
- [50] G. De La Roche, *Radio wave propagation simulation in multipath environments for the study of wireless networks*, Ph.D. thesis, INSA de Lyon, 2007.
- [51] K. Jaffres-Runser and J.-M. Gorce, *Assessment of a new indoor propagation prediction method based on a multi-resolution algorithm*, 61st Vehicular Technology Conference, IEEE, 2005.
- [52] A. Yourtchenko, *Personal communications* (2018).
- [53] J. Wong, M. Neve and K. Sowerby, *Uplink and downlink SIR analysis for base station placement*, Semiannual Vehicular Technology Conference, vol. 1, IEEE, 2003, 112–116.
- [54] A. Bahri and S. Chamberland, *On the wireless local area network design problem with performance guarantees*, Computer Networks **48** (2005), 856–866.
- [55] P. Das, N. Chakraborty and S. Allayear, *Optimal coverage of wireless sensor network using termite colony optimization algorithm*, International Conference on Electrical Engineering and Information Communication Technology, IEEE, 2015, 1–6.
- [56] F. Agelet, A. Varela, L. Alvarez-Vazquez and A. Formella, *Optimization methods for optimal transmitter locations in a mobile wireless system*, In Biennial Conference on Electromagnetic Field Computation, IEEE, 2000, 441–452.
- [57] G. Mateus, A. Loureiro and R. Rodrigues, *Optimal network design for wireless local area network*, Annals of Operations Research **106** (2001), 331–345.
- [58] C. Prommak, J. Kabara, D. Tipper and C. Charnsripinyo, *Next generation wireless LAN system design*. In Military Communications Conference, vol. 1, IEEE, 2002, 473–477.
- [59] Z. Ji, T. Sarkar and B.-H. Li, *Methods for optimizing the location of base stations for indoor wireless communications*, Transactions on Antennas and Propagation **50** (2002), 1481–1483.
- [60] K. Jaffres-Runser, *Methodologies for Wireless LAN Planning*. Ph.D. thesis, INSA de Lyon, 2005.
- [61] S. Zirazi, P. Canalda and H. Mabed and F. Spies, *Wi-Fi access point placement within stand-alone, hybrid and combined wireless positioning systems*, 4th International Conference on Communications and Electronics, IEEE, 2012, 279–284.
- [62] Z. Zhang, X. Di, J. Tian and Z. Zhu, *A multi-objective WLAN planning method*, International Conference on Information Networking, 2017, 86–91.
- [63] E. Amaldi, S. Bosio, F. Malucelli and D. Yuan, *Solving Nonlinear Covering Problems Arising in WLAN Design*, Operations Research **59** (2011), 173–187.
- [64] H. Sherali, C. Pendyala and T. Rappaport, *Optimal location of transmitters for micro-cellular radio communication system design*, Journal on selected areas in communications **14** (1996), 662–673.
- [65] H. Eldeeb, M. Arafa and M. Saidahmed, *Optimal placement of access points for indoor positioning using a genetic algorithm*, 12th International Conference on Computer Engineering and Systems, IEEE, 2017, 306–313.

- [66] X. Du and K. Yang, A map-assisted WiFi AP placement algorithm enabling mobile devices indoor positioning, *IEEE Systems Journal* **11** (2016), 1467–1475.
- [67] N. Li, J. Chen, Y. Yuan, X. Tian, Y. Han and M. Xia, A Wi-Fi indoor localization strategy using particle swarm optimization based artificial neural networks, *International Journal of Distributed Sensor Networks* **12** (2016).
- [68] T. Fruhwirth and P. Brisset, *Placing base stations in wireless indoor communication networks*, *IEEE Intelligent Systems and Their Applications*, **15** (2000), 49–53.
- [69] J. He, A. Verstak, L. Watson, C. Stinson, N. Ramakrishnan, C. Shaffer, T. Rappaport, C. Anderson, K. Bae and J. Jiang et al, *Globally optimal transmitter placement for indoor wireless communication systems*, *Transactions on Wireless Communication* **3** (2004), 1906–1911.
- [70] J. Demmel, S. Eisenstat, J. Gilbert, X. Li and J. Liu, *A supernodal approach to sparse partial pivoting*, *SIAM Journal on Matrix Analysis and Applications* **20** (1999), 720–755.
- [71] D. Vassiss, G. Kormentzas, A. Rouskas and I. Maglogiannis, *The IEEE 802.11 g standard for high data rate WLANs*, *IEEE Network* **19** (2005), 21–26.
- [72] J.-M. Gorce, K. Jaffres-Runser and G. De La Roche, *The Adaptive Multi-Resolution Frequency-Domain ParFlow (MR-FDPF) Method for Indoor Radio Wave Propagation Simulation*, Technical Report, INRIA, 2005.
- [73] T. Davis, *Direct methods for sparse linear systems*, vol. 2, SIAM, 2006.
- [74] I. Duff, A. Erisman and J. Reid, *Direct methods for sparse matrices*, Oxford University Press, 2017.
- [75] A. Hoffman, M. Martin and D. Rose, *Complexity Bounds for Regular Finite Difference and Finite Element Grids*, *SIAM Journal on Numerical Analysis* **10** (1973), 364–369.
- [76] A. George, *Nested Dissection of a Regular Finite Element Mesh*, *SIAM Journal on Numerical Analysis* **10** (1973), 345–363.
- [77] M. Garey and D. Johnson, *Computers and Intractability: A Guide to the Theory of NP-Completeness*, W. H. Freeman and Co., San Francisco, 2019.
- [78] K. Sato, T. Manabe, J. Polivka, T. Ihara, Y. Kasashima and K. Yamaki, *Measurement of the complex refractive index of concrete at 57.5 GHz*, in *IEEE Transactions on Antennas and Propagation*, **44** (1996) 35–40.
- [79] E. Jones, T. Oliphant and P. Peterson et al, *Scipy: Open source scientific tools for Python*, 2016.
- [80] IBM ILOG, *V12.8: Users manual for CPLEX*, International Business Machines Corporation, 2017.

APPENDIX

Table 13 lists, for different values of the parameter r , the sum of the objective values computed by Algorithm RH2 with this parametrization r over the 208 test cases. The third column is the spread (in %) with the average of the second column (108884). We observe that the impact of r on the performance of Algorithm RH2 is quite limited.

Value of parameter r	Sum of objective values over all instances	Relative gap to the average (over $r \in \{1.2, 1.5, 2, 3, 4\}$) performance
1.2	109020	0.12%
1.5	108730	-0.14%
2	109190	0.28%
3	108480	-0.37%
4	109000	0.11%

TABLE 13 Performance of Algorithm RH2, depending on the choice of r

How to cite this article: A. Oustry, M. Le Tilly, C. d'Ambrosio, and L. Liberti (2020), Optimal deployment of indoor wireless local area networks, *Networks*, 2020;00:1–6.